110
3-6-79

4. 2302

LA-7623-MS
Informal Report

Multiple Photon Resonances

University of California

LOS ALAMOS SCIENTIFIC LABORATORY
Post Office Box 1663 Los Alamos, New Mexico 87545

LA-7623-MS
Informal Report

UC-34a
Issued: February 1979

Multiple Photon Resonances

C. J. Elliott
B. J. Feldman

MULTIPLE PHOTON RESONANCES

by

C. J. Elliott and B. J. Feldman

ABSTRACT

A detailed theoretical analysis is presented of the interaction of intense near-resonant monochromatic radiation with an N-level anharmonic oscillator. In particular, the phenomenon of multiple photon resonance, the process by which an N-level system resonantly absorbs two or more photons simultaneously, is investigated. Starting from the Schroedinger equation, diagrammatic techniques are developed that allow the resonant process to be analyzed quantitatively, in analogy with well known two-level coherent phenomena. In addition, multiple photon Stark shifts of the resonances, shifts absent in two-level theory, are obtained from the diagrams. Insights into the nature of multiple photon resonances are gained by comparing the quantum mechanical system with classical coupled pendulums whose equations of motion possess identical eigenvalues and eigenvectors. In certain limiting cases, including that of the resonantly excited N-level harmonic oscillator and that of the equally spaced N-level system with equal matrix elements, analytic results are derived. The influence of population relaxation and phase-disrupting collisions on the multiple photon process are also analyzed; the latter by extension of the diagrammatic technique to the density matrix equations of motion.

I. INTRODUCTION

A. Background

The possibility of multiple photon resonances, the process by which an atom or molecule resonantly absorbs or emits more than one photon simultaneously, was first recognized by Goeppert-Mayer[1] early in

the development of quantum theory. Later, Besset et al.[2] and Salwen[3] examined multiple photon resonances in magnetic-spin systems by means of perturbation theory. These perturbation techniques were later adopted by Shirley[4] in treating multiple photon processes in two-level systems. Braunstein[5] has explored multiple photon absorption across the band gap in solids. More recently, interest in multiple photon processes has been stimulated by the development of short-pulse high-intensity lasers, allowing the study of such processes in atoms and molecules at optical photon frequencies[6-25]. For example, the theory of two-photon resonances has been studied in detail[26] and lately much speculation has been directed to the role of multiple photon resonances in collisionless photoabsorption and photodissociation in polyatomic molecules.

B. Approach

We will examine in some detail the dynamics of the interaction of simple nondegenerate anharmonic multilevel systems with intense quasi-resonant electromagnetic radiation. The first purpose of this treatment is to develop and gain familiarity with powerful diagrammatical techniques useful for further exploration in multiple photon theory of more complex molecular systems. The second purpose is to obtain insights into the nature of the coherent processes that arise in multilevel multiple photon absorption and how they relate to the more familiar coherent processes arising in two-level systems.

The paper is arranged in the following order. In Section IIA we will describe the multilevel model adopted for this analysis and will derive the Schroedinger Hamiltonian of the field plus multilevel system, along with the formal time-dependent solution of the corresponding Schroedinger equation. In Section IIB we will draw a useful analogy between the quantum mechanical multilevel system and a classical system of coupled pendulums. This analogue system provides insight into the nature of multiple photon resonances in the multilevel system. In Section III we will analyze the theory in the "weak-field" limit utilizing degenerate perturbation theory. A simple diagrammatic

MULTIPLE PHOTON RESONANCES

by

C. J. Elliott and B. J. Feldman

ABSTRACT

A detailed theoretical analysis is presented of the interaction of intense near-resonant monochromatic radiation with an N-level anharmonic oscillator. In particular, the phenomenon of multiple photon resonance, the process by which an N-level system resonantly absorbs two or more photons simultaneously, is investigated. Starting from the Schroedinger equation, diagrammatic techniques are developed that allow the resonant process to be analyzed quantitatively, in analogy with well known two-level coherent phenomena. In addition, multiple photon Stark shifts of the resonances, shifts absent in two-level theory, are obtained from the diagrams. Insights into the nature of multiple photon resonances are gained by comparing the quantum mechanical system with classical coupled pendulums whose equations of motion possess identical eigenvalues and eigenvectors. In certain limiting cases, including that of the resonantly excited N-level harmonic oscillator and that of the equally spaced N-level system with equal matrix elements, analytic results are derived. The influence of population relaxation and phase-disrupting collisions on the multiple photon process are also analyzed; the latter by extension of the diagrammatic technique to the density matrix equations of motion.

I. INTRODUCTION

A. Background

The possibility of multiple photon resonances, the process by which an atom or molecule resonantly absorbs or emits more than one photon simultaneously, was first recognized by Goeppert-Mayer[1] early in

the development of quantum theory. Later, Besset et al.[2] and Salwen[3] examined multiple photon resonances in magnetic-spin systems by means of perturbation theory. These perturbation techniques were later adopted by Shirley[4] in treating multiple photon processes in two-level systems. Braunstein[5] has explored multiple photon absorption across the band gap in solids. More recently, interest in multiple photon processes has been stimulated by the development of short-pulse high-intensity lasers, allowing the study of such processes in atoms and molecules at optical photon frequencies[6-25]. For example, the theory of two-photon resonances has been studied in detail[26] and lately much speculation has been directed to the role of multiple photon resonances in collisionless photoabsorption and photodissociation in polyatomic molecules.

B. Approach

We will examine in some detail the dynamics of the interaction of simple nondegenerate anharmonic multilevel systems with intense quasi-resonant electromagnetic radiation. The first purpose of this treatment is to develop and gain familiarity with powerful diagrammatical techniques useful for further exploration in multiple photon theory of more complex molecular systems. The second purpose is to obtain insights into the nature of the coherent processes that arise in multilevel multiple photon absorption and how they relate to the more familiar coherent processes arising in two-level systems.

The paper is arranged in the following order. In Section IIA we will describe the multilevel model adopted for this analysis and will derive the Schroedinger Hamiltonian of the field plus multilevel system, along with the formal time-dependent solution of the corresponding Schroedinger equation. In Section IIB we will draw a useful analogy between the quantum mechanical multilevel system and a classical system of coupled pendulums. This analogue system provides insight into the nature of multiple photon resonances in the multilevel system. In Section III we will analyze the theory in the "weak-field" limit utilizing degenerate perturbation theory. A simple diagrammatic

technique is developed in Section IIIA for a three-level prototype and is generalized to four or more levels in Section IIIB. Included in this technique is a general procedure for the determination of multiple-photon Stark shifts, whereby the energy levels and resonances of the multilevel system are shifted as a function of the strength of the applied electromagnetic field. In Section IIIC we will examine the special case of a quadratically shifted multilevel anharmonic oscillator. Exact solutions based on numerical calculations are analyzed in IIID utilizing the insights developed in this work. In Section IIIE the influence of collisions on the model is considered. Both hard collisions, that is, collisions which lead to level population depletion, and soft dephasing collisions are considered. The treatment of both soft and hard collisions is handled by means of the density matrix. The previously mentioned diagrammatic technique is employed to simplify the density matrix analysis. In the limit when soft collisions dominate, the equations of motion of the system reduce to population rate equations and, in the limit of the harmonic oscillator multilevel system, analytic solutions are obtained.

In Section IV we examine the strong field limit where the various multiple photon resonances increase in strength and width, and tend to overlap. Section IVA analyzes this regime numerically for the anharmonic oscillator. In the limit of very intense fields the behavior of the system approaches that of the harmonic oscillator. The solution to the N-level harmonic oscillator is derived in Section IVB and the well-known analytic results are examined. In Section IVC these solutions are compared with analogously derived solutions for the case of the uniformly spaced multilevel oscillator with equal dipole matrix elements. The sensitivity of the multiple photon excitation process to the relative magnitude of the single-photon dipole matrix elements is demonstrated.

II. THE MODEL

A. Formalism

We will consider the interaction of a constant-intensity monochromatic radiation field at angular frequency ω_L with a nondegenerate N-level system whose frequency spacing between adjacent levels is close to ω_L. We shall assume that finite-dipole-moment matrix elements exist only between adjacent levels. The radiation field will be treated classically, but the N-level system is by definition quantized. The system will be examined in several interesting limits analytically and, in general, numerically. In special cases, the influence of level relaxation and dephasing will also be considered. Analogies with the motion of coupled pendulum systems will clarify the physics of the coherent interactions and will suggest the results.

We will utilize the rotating-wave approximation (RWA)[27] throughout our discussion. In Appendix A we will show that the RWA adequately describes the interaction of N-levels of the combined field and oscillator system with a time-independent Hamiltonian, H. Only the combined levels of the photon-and- oscillator system that are close to each other will be considered. The others are unimportant in RWA. The oscillator-and-field energy for level i is

$$H_{ii} = E_i - (i-1)\hbar\omega_L, \quad i=1,2, \ldots N , \tag{1a}$$

and the off-diagonal elements of the Hamiltonian are

$$H_{ij} = (\delta_{i,\,j-1}+\delta_{i-1,\,j})\,\mu_{ij}\cdot E/2, \tag{1b}$$

$$i \neq j, \quad i, j=1, 2, \ldots N.$$

where the applied field is given by

$$E_A = Ee^{i\omega_L t} + C.C. \tag{1c}$$

We shall refer to this Hamiltonian as the Schroedinger Hamiltonian because it is the time-independent Hamiltonian of the oscillator plus field.

The time-dependent solution of the Schroedinger Hamiltonian is determined by standard techniques. The eigenvalues λ_k are given by

$$|H_{mn} - \lambda_k \delta_{mn}| = 0. \tag{2}$$

Corresponding to each value λ_k there is an eigenvector ψ^k and a solution of the time-dependent Schroedinger equation

$$\psi^k \exp\left(\frac{i\lambda_k t}{\hbar}\right). \tag{3}$$

The general solution is a superposition of these N-time-evolved eigenvectors, the precise linear combination of which is determined by the appropriate boundary conditions at t=0. For our purpose, we shall assume that the system is entirely in the ground state at t=0.

We shall now examine two limiting cases of these equations. The first pertains to weak fields, i.e., when the off-diagonal matrix elements are small compared to the diagonal matrix elements except for the two levels n_L and n_u, where the diagonal matrix elements are nearly zero:

$$|\mu_{i,\,i+1}\cdot E| \ll E_j - (j-1)\hbar\omega_L \quad , \tag{4}$$

for all i, and all $j \neq n_L, n_u$.

In this weak-field limit, degenerate perturbation theory can be applied. The second limit pertains if the off-diagonal matrix elements are large compared to the diagonal matrix elements.

$$|\mu_{i,i+1}\cdot E| \gg E_j - (j-1)\hbar\omega_L \quad . \tag{5}$$

In this case where the detunings are small compared to the induced broadening the diagonal elements can be neglected and the system acts like a harmonic oscillator.

B. Pendulum Analogy

The properties of the quantum-mechanical system may be understood by examining a coupled N-pendulum system, shown in Fig. 1 . We show in Appendix B that choosing appropriate lengths and spring constants, the eigenvalues and eigenvectors of this classical system are precisely those associated with the N-level quantum-mechanical system. Note, however, that the physical analogue is not exact. The pendulum problem is second order in time, whereas the quantum-mechanical problem is first order. Even so, much insight can be gained by studying this analogue.

The system of pendulums with weak springs (Fig. 1) exhibits most clearly the analogue of multiple photon resonances. In this particular figure, chosen to simulate a five-photon resonance, the first pendulum and the sixth are of the same length. Consider the consequences of plucking the left-most pendulum to the left and releasing it. Initially it oscillates at a resonance frequency, providing a slightly off-resonance driving force for the second pendulum. The second pendulum responds weakly, but does provide a slight driving force to the third pendulum. At the sixth pendulum the driving force is extremely weak, but on resonance. Consequently, because an oscillation will grow without bound with a resonant driving force, the sixth pendulum will gradually acquire a significant fraction of the total energy of the system.

The same type of analysis holds for the quantum-mechanical case. However, the frequencies of the pendulums are not analogous to the energy levels of the system. For example, in the special case of a harmonic oscillator the pendulums are all of equal length and have the same stand-alone frequency, whereas the quantum levels increase linearly in energy. In the quantum case the amplitude of state n alone does not drive state n+1. Instead it is the product of the oscillating electric field and the amplitude of state n. Each time we move from one level to the next we are dealing with a higher frequency harmonic. For a six level system the driving force is fifth harmonic and the resonance condition demands that this fifth harmonic be the same as ω_{61}

as contrasted to the pendulums that simply require the first and sixth pendulum be nearly the same height.

We may now enumerate the multiple photon resonances in the quantum-mechanical multilevel system. A distinct resonance is associated with each pair of levels. For upper level n_u and lower level n_L, $n_u - n_L$ photons are required. The resonance condition for the laser frequency ω_L is (except for small coupling corrections) given by

$$\omega_L \cong (\omega_{n_u} - \omega_{n_L})/(n_u - n_L) \quad . \tag{6}$$

Under some conditions, not all these resonances will show up. When the field is weak, only the resonances connected to the ground state are important. As the field increases the other resonances come into play.

III. WEAK-FIELD LIMIT

A. Three-Level Prototype

We now consider a three-level system where $2\omega_L \cong \omega_{31}$.[28] Because of the resonance condition between the first and the third level, we must employ degenerate perturbation theory. In first-order theory, the first level is coupled to the second and the second to the third, but not the first to the third. Thus, the degeneracy that requires an interaction of the first and third level is not broken. To remove the degeneracy, we must resort to second-order perturbation theory. In general for an N-photon transition, N'th-order perturbation theory is required to couple the levels. This again is obvious by looking at the pendulum model where the coupling of a pendulum to its neighbor results in an amplitude weaker by one order in the coupling parameter.

The degenerate perturbation theory can be applied in various ways. Time-dependent perturbation theory can be used, but it is only useful for times much shorter than Ω_R^{-1} where Ω_R is the effective Rabi frequency[29] (to be defined below). We desire a perturbation theory which gives expansions that are uniform in time. Standard time-independent perturbation theory can be applied with relative ease if Schwinger projection operators[30] or Heitler transformations[31] are used. For this work, we have developed the following simple diagrammatic technique.

The diagrammatic technique presented here represents a powerful tool for exploring multiple photon processes in more complex multilevel systems. The technique is first applied to a three-level system to gain familiarity with methodology. The diagrams and their interpretations are then applied to the analysis of four-and higher-level systems. Later these techniques are extended to density matrix equations for an N-level system where relaxation and dephasing collisions are included.

For the three-level system, the Schroedinger equation in RWA is

$$\frac{\hbar\partial}{i\partial t}\psi = \hbar \begin{vmatrix} 0 & a & 0 \\ a^* & \Omega_{21} & b \\ 0 & b^* & \Omega_{31} \end{vmatrix} \psi \quad , \tag{7}$$

where for our nearly harmonic system

$$\hbar\Omega_{jk} = E_j - E_k - (j-k)\hbar\omega_L = H_{jj} - H_{kk} \quad , \tag{8}$$
$$\hbar a = H_{12}, \quad \hbar b = H_{23}$$

The parameter Ω_{21} measures the departure from a harmonic system. The resonance detuning Ω_{31} is nearly zero for resonance, resulting in a matrix with nearly degenerate eigenvalues. The Rabi frequency $\omega_R = 2H_{12}/\hbar$ couples the levels, is small compared to Ω_{21}.

To facilitate the interpretation of the diagrams we will use the interaction Hamiltonian in which we eliminate the diagonal matrix elements by transformation, and therefore, do not have to interpret them. Later, in evaluating the diagrams, it will be advantageous to return to the Schroedinger representation. The interaction representation is indicated by a subscript I.

$$\frac{\hbar}{i}\frac{\partial}{\partial t}\psi_I = H_I\,\psi_I \quad , \tag{9a}$$

where

$$H_I = \exp\left(\frac{-iH_0t}{\hbar}\right)(H - H_0)\exp\left(\frac{iH_0t}{\hbar}\right) , \tag{9b}$$

and

$$H_0 = \begin{bmatrix} H_{11} & 0 & 0 \\ 0 & H_{22} & 0 \\ 0 & 0 & H_{33} \end{bmatrix}, \quad H_I = \begin{bmatrix} 0 & \alpha & 0 \\ \alpha^* & 0 & \beta \\ 0 & \beta^* & 0 \end{bmatrix} , \tag{9c}$$

where

$$\alpha = \hbar a \exp\,(i\Omega_{21}t),\ \beta = \hbar b \exp(i\Omega_{32}t)\ . \tag{9d}$$

In this form the interaction Hamiltonian is first order in the field.

We now introduce diagrams that are different from the Feynmann type utilized by Ward and Wallace[32], ours being tailored for multiple photon resonances. The advantages of using diagrams rather than, for example, projection operators are the ease of visualization and the ability to restrict the diagrams only to those required for a given process.

A single dot in a level is used to represent a pure state in that level. If more than one dot appears we have a mixed state. Because the degeneracy of the two states in a two-photon resonance results in an admixture of the wavefunctions, we represent the lowest significant-order wave-function corresponding to a two-photon resonance as

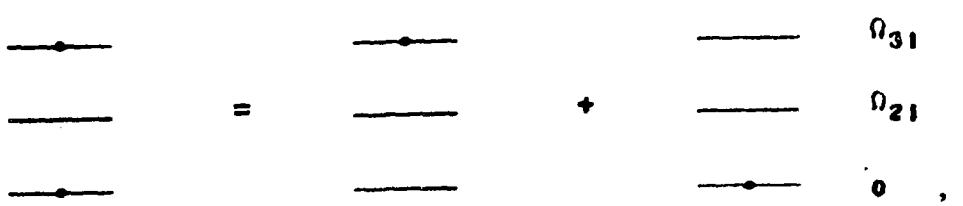

(10)

where the energy or angular frequency associated with each state is indicated to the right of the level. Even a mixed state can be easily represented in one diagram because the decomposition sequence is clearly indicated.

The interaction Hamiltonian relates the diagrams by the following rules:

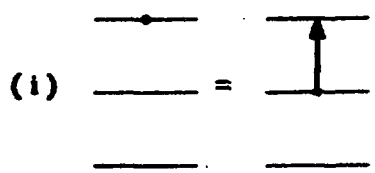

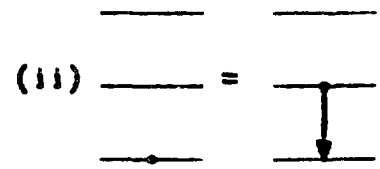

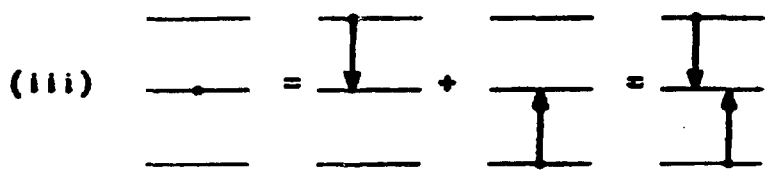

(11)

The dot represents a known amplitude and an arrow with a dot at its tail represents the contribution to the level at the arrow's end due to the known amplitude. For instance, according to (i), if we know the amplitude of the middle level as a function of time, we can find the amplitude of the upper level as a function of time through the matrix element of the Hamiltonian. In instances (ii) and (iii) each level is

assumed to have a harmonic time dependence because we are seeking eigenvectors and eigenvalues. We are <u>not</u> solving an initial value problem.

Formally we have

$$\psi_I = \frac{i}{\hbar}\int dt H_I \psi_I \quad , \tag{12}$$

where the right-hand sides (RHS) of Eq. (11i)-(11iii) are represented by The RHS of Eq. (12). Note, that each arrow represents the contribution to the state at its head; and not a negative contribution to the state at its tail. Conservation of probability can be demonstrated by writing the complete Hamiltonian for a single diagram

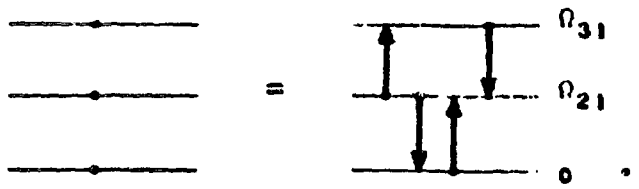

(13)

Arrows pointing in the reverse direction connect the same levels for hermitian Hamiltonians and thereby permit conservation of probability.

We may iterate Eq. (12), by replacing ψ_I of the RHS by the left-hand side (LHS). This corresponds to replacing the dot at the tail of the arrow by another arrow whose head is at the position of the replaced dot and with a dot at its end. For instance,

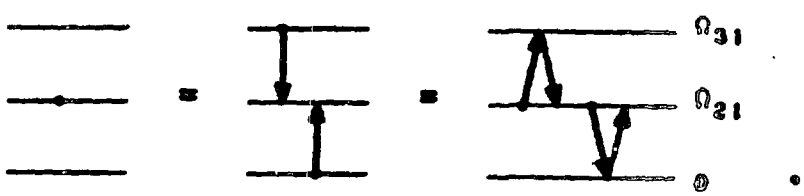

(14)

where the diagrams with successive arrows connected head-to-tail are interpreted as iterated integrals. For the type of expansion we require in perturbation theory we use

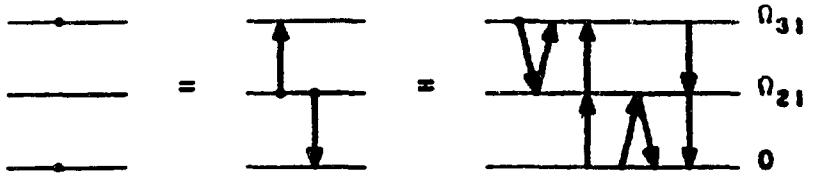

(15)

where we have not replaced the upper dot by Eq. (11i) in the last step of the evaluation. In the following procedure we will never replace the upper- or lower-state dot except in the very first step. We are singling out the upper and lower states as is done in degenerate perturbation theory using projection operators.

For this three-level system we do not neglect any diagrams, as we must for four- or higher-level systems. To find the mixed state representing the wavefunction amplitudes of lowest significant order for the upper and lower levels, B_u and B_L, of the interaction representation, with our rules we obtain

$$B_u = \frac{i}{\hbar}\int dt\beta \frac{i}{\hbar}\int dt\ \beta^*\ B_u + \frac{i}{\hbar}\int dt\ \beta \frac{i}{\hbar}\int dt\ \alpha\ B_L\ , \tag{16a}$$

$$B_L = \frac{i}{\hbar}\int dt\ \alpha^* \frac{i}{\hbar}\int dt\ \alpha B_L + \frac{i}{\hbar}\int dt\ \alpha^* \frac{i}{\hbar}\int dt\ \beta^*\ B_u\ . \tag{16b}$$

assumed to have a harmonic time dependence because we are seeking eigenvectors and eigenvalues. We are <u>not</u> solving an initial value problem.

Formally we have

$$\psi_{\mathrm{I}} = \frac{i}{\hbar}\int dt H_{\mathrm{I}}\psi_{\mathrm{I}} \quad , \tag{12}$$

where the right-hand sides (RHS) of Eq. (11i)-(11iii) are represented by The RHS of Eq. (12). Note, that each arrow represents the contribution to the state at its head; and not a negative contribution to the state at its tail. Conservation of probability can be demonstrated by writing the complete Hamiltonian for a single diagram

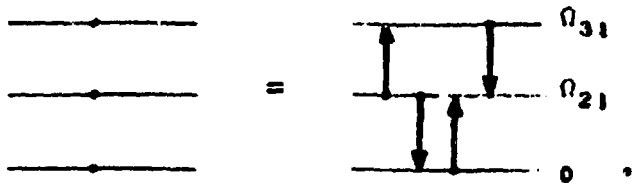

(13)

Arrows pointing in the reverse direction connect the same levels for hermitian Hamiltonians and thereby permit conservation of probability.

We may iterate Eq. (12), by replacing ψ_{I} of the RHS by the left-hand side (LHS). This corresponds to replacing the dot at the tail of the arrow by another arrow whose head is at the position of the replaced dot and with a dot at its end. For instance,

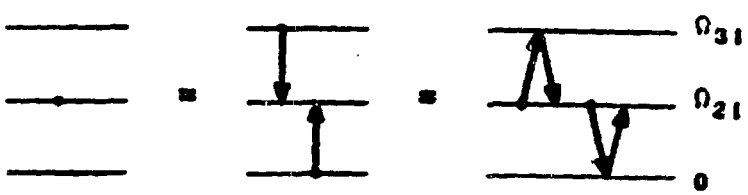

(14)

where the diagrams with successive arrows connected head-to-tail are interpreted as iterated integrals. For the type of expansion we require in perturbation theory we use

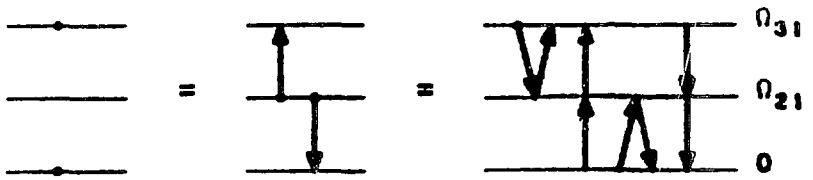

(15)

where we have not replaced the upper dot by Eq. (11i) in the last step of the evaluation. In the following procedure we will never replace the upper- or lower-state dot except in the very first step. We are singling out the upper and lower states as is done in degenerate perturbation theory using projection operators.

For this three-level system we do not neglect any diagrams, as we must for four- or higher-level systems. To find the mixed state representing the wavefunction amplitudes of lowest significant order for the upper and lower levels, B_u and B_L, of the interaction representation, with our rules we obtain

$$B_u = \frac{i}{\hbar}\int dt\beta \frac{i}{\hbar}\int dt\ \beta^*\ B_u + \frac{i}{\hbar}\int dt\ \beta \frac{i}{\hbar}\int dt\ \alpha\ B_L\ , \tag{16a}$$

$$B_L = \frac{i}{\hbar}\int dt\ \alpha^* \frac{i}{\hbar}\int dt\ \alpha B_L + \frac{i}{\hbar}\int dt\ \alpha^* \frac{i}{\hbar}\int dt\ \beta^*\ B_u\ . \tag{16b}$$

assumed to have a harmonic time dependence because we are seeking eigenvectors and eigenvalues. We are <u>not</u> solving an initial value problem.

Formally we have

$$\psi_I = \frac{i}{\hbar}\int dt H_I \psi_I \quad , \tag{12}$$

where the right-hand sides (RHS) of Eq. (11i)-(11iii) are represented by The RHS of Eq. (12). Note, that each arrow represents the contribution to the state at its head; and not a negative contribution to the state at its tail. Conservation of probability can be demonstrated by writing the complete Hamiltonian for a single diagram

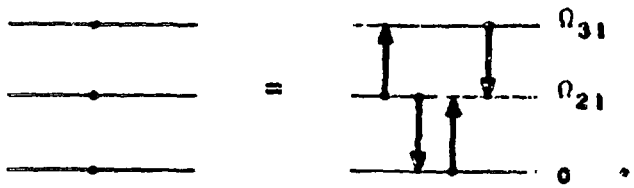

(13)

Arrows pointing in the reverse direction connect the same levels for hermitian Hamiltonians and thereby permit conservation of probability.

We may iterate Eq. (12), by replacing ψ_I of the RHS by the left-hand side (LHS). This corresponds to replacing the dot at the tail of the arrow by another arrow whose head is at the position of the replaced dot and with a dot at its end. For instance,

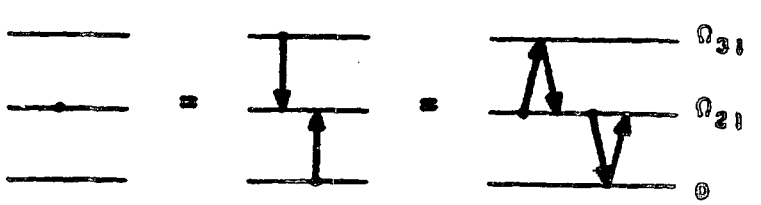

(14)

where the diagrams with successive arrows connected head-to-tail are interpreted as iterated integrals. For the type of expansion we require in perturbation theory we use

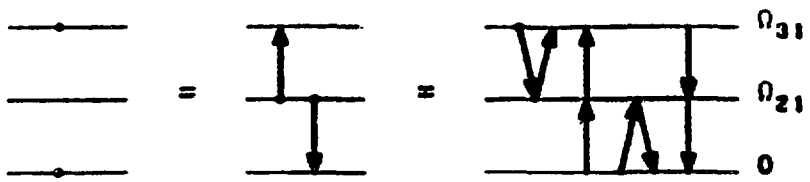

(15)

where we have not replaced the upper dot by Eq. (11i) in the last step of the evaluation. In the following procedure we will never replace the upper- or lower-state dot except in the very first step. We are singling out the upper and lower states as is done in degenerate perturbation theory using projection operators.

For this three-level system we do not neglect any diagrams, as we must for four- or higher-level systems. To find the mixed state representing the wavefunction amplitudes of lowest significant order for the upper and lower levels, B_u and B_L, of the interaction representation, with our rules we obtain

$$B_u = \frac{i}{\hbar}\int dt\beta \frac{i}{\hbar}\int dt\ \beta^*\ B_u + \frac{i}{\hbar}\int dt\ \beta \frac{i}{\hbar}\int dt\ \alpha\ B_L\ , \tag{16a}$$

$$B_L = \frac{i}{\hbar}\int dt\ \alpha^* \frac{i}{\hbar}\int dt\ \alpha B_L + \frac{i}{\hbar}\int dt\ \alpha^* \frac{i}{\hbar}\int dt\ \beta^*\ B_u\ . \tag{16b}$$

assumed to have a harmonic time dependence because we are seeking eigenvectors and eigenvalues. We are <u>not</u> solving an initial value problem.

Formally we have

$$\psi_{\mathrm{I}} = \frac{i}{\hbar}\int dt H_I \psi_I \quad , \tag{12}$$

where the right-hand sides (RHS) of Eq. (11i)-(11iii) are represented by The RHS of Eq. (12). Note, that each arrow represents the contribution to the state at its head; and not a negative contribution to the state at its tail. Conservation of probability can be demonstrated by writing the complete Hamiltonian for a single diagram

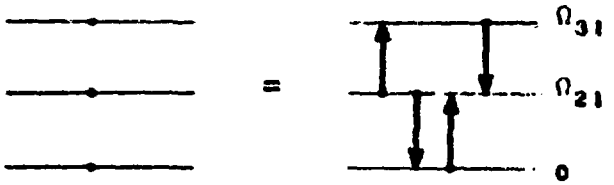

(13)

Arrows pointing in the reverse direction connect the same levels for hermitian Hamiltonians and thereby permit conservation of probability.

We may iterate Eq. (12), by replacing ψ_I of the RHS by the left-hand side (LHS). This corresponds to replacing the dot at the tail of the arrow by another arrow whose head is at the position of the replaced dot and with a dot at its end. For instance

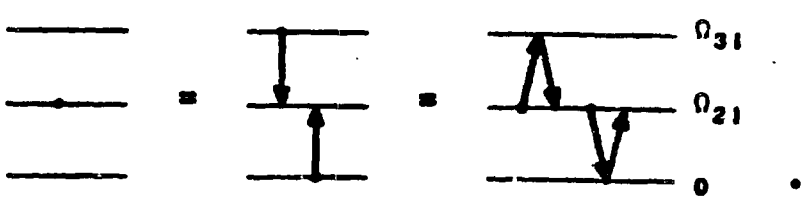

(14)

where the diagrams with successive arrows connected head-to-tail are interpreted as iterated integrals. For the type of expansion we require in perturbation theory we use

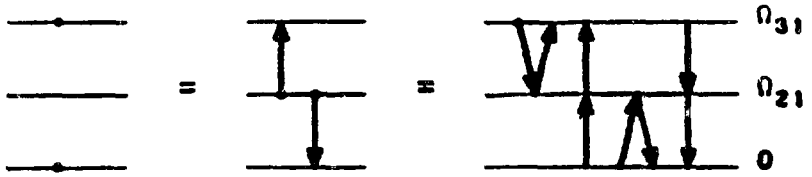

(15)

where we have not replaced the upper dot by Eq. (111) in the last step of the evaluation. In the following procedure we will never replace the upper- or lower-state dot except in the very first step. We are singling out the upper and lower states as is done in degenerate perturbation theory using projection operators.

For this three-level system we do not neglect any diagrams, as we must for four- or higher-level systems. To find the mixed state representing the wavefunction amplitudes of lowest significant order for the upper and lower levels, B_u and B_L, of the interaction representation, with our rules we obtain

$$B_u = \frac{i}{\hbar}\int dt\beta \frac{i}{\hbar}\int dt\ \beta^*\ B_u + \frac{i}{\hbar}\int dt\ \beta \frac{i}{\hbar}\int dt\ \alpha\ B_L\ , \tag{16a}$$

$$B_L = \frac{i}{\hbar}\int dt\ \alpha^* \frac{i}{\hbar}\int dt\ \alpha B_L + \frac{i}{\hbar}\int dt\ \alpha^* \frac{i}{\hbar}\int dt\ \beta^*\ B_u\ . \tag{16b}$$

assumed to have a harmonic time dependence because we are seeking eigenvectors and eigenvalues. We are <u>not</u> solving an initial value problem.

Formally we have

$$\psi_{\mathcal{I}} = \frac{i}{\hbar}\int dt H_I \psi_I \quad , \tag{12}$$

where the right-hand sides (RHS) of Eq. (11i)-(11iii) are represented by The RHS of Eq. (12). Note, that each arrow represents the contribution to the state at its head; and not a negative contribution to the state at its tail. Conservation of probability can be demonstrated by writing the complete Hamiltonian for a single diagram

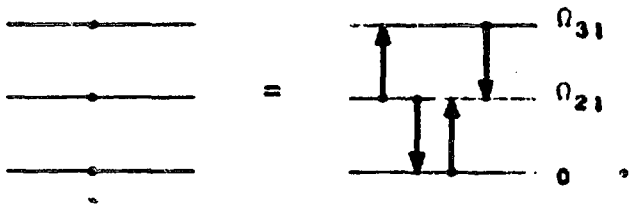

(13)

Arrows pointing in the reverse direction connect the same levels for hermitian Hamiltonians and thereby permit conservation of probability.

We may iterate Eq. (12), by replacing ψ_I of the RHS by the left-hand side (LHS). This corresponds to replacing the dot at the tail of the arrow by another arrow whose head is at the position of the replaced dot and with a dot at its end. For instance,

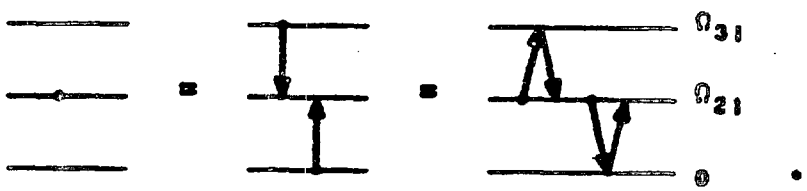

(14)

where the diagrams with successive arrows connected head-to-tail are interpreted as iterated integrals. For the type of expansion we require in perturbation theory we use

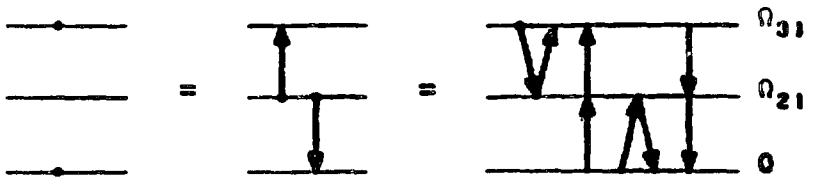

(15)

where we have not replaced the upper dot by Eq. (11i) in the last step of the evaluation. In the following procedure we will never replace the upper- or lower-state dot except in the very first step. We are singling out the upper and lower states as is done in degenerate perturbation theory using projection operators.

For this three-level system we do not neglect any diagrams, as we must for four- or higher-level systems. To find the mixed state representing the wavefunction amplitudes of lowest significant order for the upper and lower levels, B_u and B_L, of the interaction representation, with our rules we obtain

$$B_u = \frac{i}{\hbar}\int dt\beta \frac{i}{\hbar}\int dt\ \beta^*\ B_u + \frac{i}{\hbar}\int dt\ \beta \frac{i}{\hbar}\int dt\ \alpha\ B_L\ , \tag{16a}$$

$$B_L = \frac{i}{\hbar}\int dt\ \alpha^* \frac{i}{\hbar}\int dt\ \alpha B_L + \frac{i}{\hbar}\int dt\ \alpha^* \frac{i}{\hbar}\int dt\ \beta^*\ B_u\ . \tag{16b}$$

The right form for the iterated integrals can be established easily. For instance, the second term in Eq. (16a) follows by solving for B_u, where

$$\frac{\hbar \partial B}{i \partial t^2} = H_{I_{23}} B_u \ ,$$

and

$$\frac{\hbar \partial B'_u}{i \partial t} = H_{I_{32}} B_2 \ ,$$

and where H_{Iij} are the matrix elements of the H_I matrix given in Eq. (9c).

One way to proceed at this point would be to evaluate the above expressions using the definitions of α and β. This procedure is quite adequate, but the bookkeeping is somewhat more obvious if we factor out the time dependence of the wavefunction from the beginning. Rather than generate resonance denominators by integrals over time as in Eq. (16), we may deal directly with energy differences.

By replacing $\partial\psi/\partial t$ in Eq. (7) by $i\nu\psi$, the eigenvalue problem which we are now solving can be written

$$\begin{vmatrix} -\nu & a & 0 \\ a^* & \Omega_{21}-\nu & b \\ 0 & b^* & \Omega_{31}-\nu \end{vmatrix} \psi_0 = 0 \ , \qquad (17)$$

where $\psi = \psi_0 \exp(i\nu t)$. Our method below is in step-to-step agreement with the interaction approach. Denoting the amplitudes of ψ_0 by a_1, a_2, a_3, we have for the diagram from $3 \to 2 \to 3$

$$(H_{33} - \nu)a_3' + H_{32}a_2 = 0,$$

and

$$(H_{22} - \nu)a_2 + H_{23}a_3 = 0 \quad , \tag{18}$$

where a_3' is the contribution to a_3 due to this diagram. Hence

$$a'_3 = \frac{H_{32}}{\nu - H_{33}} \frac{H_{23}}{\nu - H_{22}} a_3 \quad . \tag{19}$$

Likewise the diagram $1 \to 2 \to 3$ gives

$$a''_3 = \frac{H_{21}}{\nu - H_{22}} \frac{H_{32}}{\nu - H_{33}} a_1 \quad , \tag{20}$$

The right form for the iterated integrals can be established easily. For instance, the second term in Eq. (16a) follows by solving for B_u, where

$$\frac{\hbar \partial B}{i \partial t^2} = H_{I_{23}} B_u \ ,$$

and

$$\frac{\hbar \partial B'_u}{i \partial t} = H_{I_{32}} B_2 \ ,$$

and where H_{Iij} are the matrix elements of the H_I matrix given in Eq. (9c).

One way to proceed at this point would be to evaluate the above expressions using the definitions of α and β. This procedure is quite adequate, but the bookkeeping is somewhat more obvious if we factor out the time dependence of the wavefunction from the beginning. Rather than generate resonance denominators by integrals over time as in Eq. (16), we may deal directly with energy differences.

By replacing $\partial\psi/\partial t$ in Eq. (7) by $i\nu\psi$, the eigenvalue problem which we are now solving can be written

$$\begin{vmatrix} -\nu & a & 0 \\ a^* & \Omega_{21}-\nu & b \\ 0 & b^* & \Omega_{31}-\nu \end{vmatrix} \psi_0 = 0 \ , \qquad (17)$$

where $\psi = \psi_0 \exp(i\nu t)$. Our method below is in step-to-step agreement with the interaction approach. Denoting the amplitudes of ψ_0 by a_1, a_2, a_3, we have for the diagram from $3 \to 2 \to 3$

$$(H_{33} - \nu)a_3' + H_{32}a_2 = 0,$$

and

$$(H_{22} - \nu)a_2 + H_{23}a_3 = 0 \quad , \tag{18}$$

where a_3' is the contribution to a_3 due to this diagram. Hence

$$a'_3 = \frac{H_{32}}{\nu - H_{33}} \frac{H_{23}}{\nu - H_{22}} a_3 \quad . \tag{19}$$

Likewise the diagram $1 \to 2 \to 3$ gives

$$a''_3 = \frac{H_{21}}{\nu - H_{22}} \frac{H_{32}}{\nu - H_{33}} a_1 \quad , \tag{20}$$

where a_3'' is the contribution due to this diagram and $a_3 = a_3' + a_3''$. Carrying out a similar procedure for level 1 we find

$$\begin{vmatrix} \frac{H_{21}H_{12}}{(\nu-H_{22})(\nu-H_{11})} & \frac{H_{21}H_{32}}{(\nu-H_{22})(\nu-H_{11})} \\ \frac{H_{23}H_{12}}{(\nu-H_{33})(\nu-H_{22})} & \frac{H_{23}H_{32}}{(\nu-H_{22})(\nu-H_{33})} \end{vmatrix} \begin{vmatrix} a_1 \\ a_3 \end{vmatrix} = \begin{vmatrix} a_1 \\ a_3 \end{vmatrix} , \tag{21}$$

which may be put in the convenient form

$$\begin{vmatrix} \frac{H_{21}H_{12}}{\nu-H_{22}} + H_{11}, \frac{H_{21}H_{32}}{\nu-H_{22}} \\ 1 \\ \frac{H_{23}H_{12}}{\nu-H_{22}} \quad , \frac{H_{23}H_{32}}{\nu-H_{22}} + H_{33} \end{vmatrix} \begin{vmatrix} a_1 \\ a_3 \end{vmatrix} = \nu \begin{vmatrix} a_1 \\ a_3 \end{vmatrix} \tag{22}$$

These may be verified directly from Eq. (16) with an assumed time dependence of

$$B_u = a_3 \exp[i(H_{33}-\nu)t/\hbar], \; B_L = a_1 \exp[i(H_{11}-\nu)t/\hbar] \quad .$$

Because, as shall see, $|\nu| << |H_{22}|$, Eq. (22) represents for the weak-

limit, a reduction of the three-level problem to an equivalent two-level problem. The energy of the original Hamiltonian H_{11} of level 1 is perturbed by the Stark shift $-H_{21}H_{12}/H_{22}$, that of level 2 by $-H_{23}H_{32}/H_{22}$, and the effective Rabi frequency, Ω_R, is $|2H_{12}H_{23}/(\hbar H_{22})|$. These results are in accord with those of Ref. (26).

By using our procedure we could, in principle, derive the diagram of Eq. (22) from that of Eq. (15), together with the corresponding two-level equations for an N-level system. In Eq. (22) we keep the diagonal matrix elements and add terms that may be constructed by the following rules:

(i) The effective matrix element for a diagram in going from i_1 to i_2 to $\ldots i_n$ is

$$\frac{H_{i_2,i_1}H_{i_3,i_2}\cdots H_{i_N,i_{N-1}}}{(\upsilon-H_{i_2,i_2})(\upsilon-H_{i_3,i_3})\ldots(\upsilon-H_{i_{N-1},i_{N-1}})} \qquad (23)$$

(ii) All matrix elements starting at i_1 and ending at i_n are added (i_1, i_n = upper or lower state level numbers).

B. The Four-Level Case

We are now ready to examine the four-level case. The equation analogous to the first part of Eq. (11) is

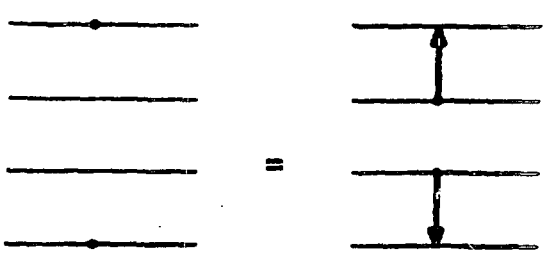

(24)

As before, we replace the middle two levels by their equivalents giving

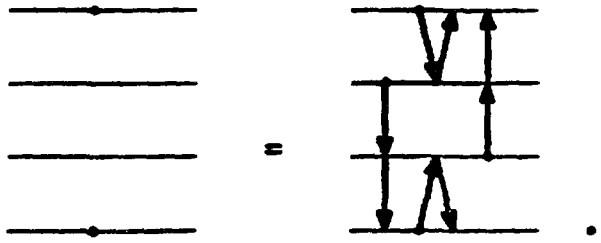

(25)

We then replace the two terms originating on the middle two levels by their equivalents once more so that the upper and lower levels will be connected, giving

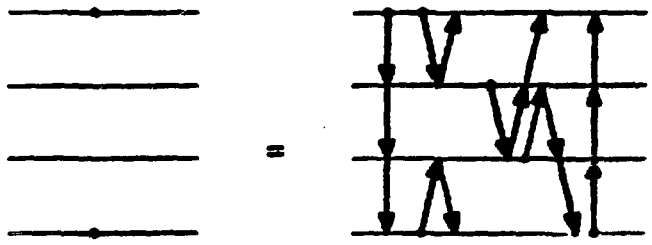

(26)

Next, we note that for the mixed-state eigenvector, to lowest significant order, the upper-and lower-level amplitudes are of the order of unity and the middle two levels are of the order (Ω_R/Ω) where Ω is the minimum of the nonresonant detunings. We also note that all the diagrams originating on the middle levels and ending on the upper or lower level are three legs long. These diagrams are thus of order $(\Omega_R/\Omega)^4$. We may formally write

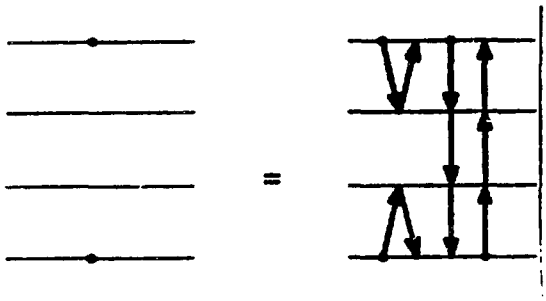

(27)

We may now proceed to write the effective two-level Hamiltonian, as we did before, by using the rules outlined above. The upper and lower levels are both Stark-shifted by terms that are quadratic in the field, i.e., two-photon terms, and the levels are coupled by a three-photon term. However, rather than write the equations for this case we will consider a more complete case in Appendix C.

The general case is governed by the above rules. Multiple-photon Stark shifts of each of the levels will involve an even number of photons whose total is less than, or equal to, N, the number of photons of the transition. The energy level with its Stark shift can then be represented by a power series in intensity. Based on generalization of the above example, important diagrams which give a Stark shift larger than or comparable to, the linewidth of an N-photon transition are determined by the following rule:

(iii) Every diagram having N-legs or less, originating and terminating on the same level (either the upper or lower), must be included, but no intermediate states can be the same as the originating or terminating level. These rules are applied to a $1 \rightarrow 6$ transition in a 10-level system in Appendix C.

C. Quadratic Hamiltonian

The Hamiltonian in Eq. (1) does not give any specific distribution of energy levels in our system. Here we consider the special case of the anharmonic oscillator, with harmonic-oscillator matrix elements but with the energy of the levels shifted quadratically from that of the harmonic oscillator. The Hamiltonian then takes the form

$$H_{mn} = 0.5\hbar\omega_R[\sqrt{m}\delta_{m,n-1} + \sqrt{n}\delta_{m-1,n}] + \delta_{m,n}\hbar(n-1)[\omega_{21}-\omega_L - (n-2)\Delta/2]. \tag{28}$$

The anharmonic parameter Δ is given by

$$\Delta = \omega_{23} - \omega_{12} \quad . \tag{29}$$

With this anharmonicity, the single resonance frequency of the harmonic oscillator becomes split into many components. Except for Stark shifts, the single-step resonances for the N-level system are

$$\omega_L = \omega_{21} - (n - 1)\,\Delta \quad . \tag{30}$$

There are also important multiple-photon resonances, which we have mentioned previously. For this particular anharmonic oscillator, the multiple-photon resonances are degenerate. The resonances (except for Stark shifts) may be computed to be of the form

$$\omega_L \cong \omega_{21} + R_{n_u n_L}\,\Delta \quad , \tag{31}$$

where R is the positive number of anharmonic units, Δ, above (negative for below) the first single-photon resonance of the system. The values of R are shown in Fig. 2 for a ten-level system. We see that in our ten-level system the multiple-photon resonances have a degeneracy of 1 to 5, and all fall on or below ω_{21}.

Under some conditions, not all of these resonances will appear. In a weak field, only the resonances connected to the ground state are important. As the field increases the other resonances emerge.

D. Numerical Results

The resonances described above can easily be examined numerically. In these calculations we must choose a frequency grid, a pulse length, and an intensity. In addition, parameters corresponding to the modeled quantum-mechanical system must be specified. For the purposes of the present calculations we have taken $\Delta = 7.5 \cdot 10^{11}$ rad/s and $(\mu_{12})_x = 0.3$ Debyes, and a pulse length of 1.0 ns.

In Fig. 3 we see our resonances for a grid spacing of $2.67 \cdot 10^{-3}\Delta$ and an intensity of 40MW/cm^2 giving $\omega_R = 0.116\Delta$. Because of the rapid oscillations in frequency the data could not be traced as computed. We therefore removed the high-frequency oscillations by convoluting the data with a triangular weight function having a half-width of 20 grid points. The data displayed in Fig. 3 thus are similar to those taken by an instrument with a resolution of $\Delta/20$.

It appears that a doublet occurs near $\omega_L = \omega_{21}$; however, this structure is a two-level effect and occurs because of our particular pulse length. The population of level 2 oscillates between zero and unity as

$$[\omega_R \sin(0.5\omega_{DR}t)/\omega_{DR}]^2 \quad , \tag{??}$$

where the detuned effective Rabi frequency is

$$\omega_{DR} = [\omega_R^2 + (\omega_L - \omega_{21})^2]^{1/2} \quad . \tag{33}$$

We selected a time when the upper level was not at peak amplitude. Shifting the frequency on either side of ω_{21} allows the amplitude to peak and, thus, gives rise to the apparent doublet structure. This two level approximation explains the bulk of Fig. 3 except for the multiple photon resonances.

We can see evidence of resonances in Fig. 3 at $\omega_L-\omega_{21} = 0$, -0.5Δ, $-\Delta$, and -1.5Δ which correspond to $1\rightarrow 2$, $1\rightarrow 3$, $1\rightarrow 4$, and $1\rightarrow 5$ resonances, respectively. The $-\Delta$ and -1.5Δ resonances are degenerate as is seen in Fig. 2 ; however, the other possible interpretations i.e. $2\rightarrow 3$ and $2\rightarrow 4$ involve states which do not initiate on the ground state, and we do not expect these excited states to be appreciably populated at this intensity except near $_L = _{21}$.

We can see additional resonances at a higher intensity of $4GW/cm^2$ ($\omega_R = 1.16\Delta$). In Fig. 4 we can see most of the previous resonances and, in addition, a resonance at $\omega_L - \omega_{21} = -2\Delta$. The character of the $\omega_L = \omega_{21}$ resonance has clearly changed and the structure analogous to the doublet of Fig. 4 has become more complicated, although the wing of the curve ($\omega>\omega_{21} + \Delta/2$) is still described by a two-level model. The weak-field limit, thus, applies at $\omega_R > \Delta$ if we are in the wings of the curve.

Next, we investigate the resonance seen in Fig. 4 which occurs at $\omega_L - \omega_{21} = -2\Delta$. At this high intensity we can not rule out a resonance from an excited state such as $2\rightarrow 5$ or $3\rightarrow 4$, but we highly suspect it to be a $1\rightarrow 6$ resonance. To determine which, we look at the time evolution of the probabilities of being in each state. These states are shown in Fig. 5 , which plots the probability of being in state 1 between 1 and 2 and that of being in state 2 between 2 and 3, etc. The ground state starts at unity and decreases to a minimum of nearly zero. At this minimum, level 6 is at its peak: it anticorrelates, just as in the pendulum case where the amplitudes are weak between the first and sixth pendulum. The angular frequency of the oscillation Ω_R we call the effective Rabi frequency when we are on resonance, as we are here. The reasons for not achieving unity probability of level 6; for the structure on the level-6 and level-1

probability curves; and for the excitation of levels 5 and 2 are all related. The weak-field limit, which presumes $\omega_R << \Delta$, is just beginning to break down at $\omega_R = 1.16\Delta$. It begins to break down at such a high ω_R because we are nearly in the wing of the $1 \mapsto 2$ resonance so that level 2 is just beginning to be populated at this frequency and intensity.

The shape of the $1 \mapsto 6$ resonance line is shown in detail in Fig. 6 . Here we look at the resonance with a grid spacing of $10^{-4}\Delta$, which is more than adequate for resolution. Rather than averaging the rapidly oscillating curve over a small frequency interval as we did before, we have plotted the population maximum with respect to time. The shape of the curve in Fig. 6 is nearly Lorentzian, with a slight shift, nearly centered on $\omega_L = \omega_{21} - 2\Delta$.

In Fig. 7 we examine the half-width and shift of this resonance over a wide intensity range. The width varies as $I^{5/2}$, and the shift as I^5. For comparison we plot the difference of the two smallest eigenvalues that occur at $\omega_L = \omega_{21} - 2\Delta$ as well as their sum. The difference of the two eigenvalues gives the effective Rabi frequency Ω_R, whereas their sum gives the sum of the Stark shifts for the upper and lower level. As we expected on the basis of the equivalent two-level model, the width of the resonance is one-fifth the effective Rabi frequency giving the $I^{5/2}$ dependence. Details of the reduction of the ten-level system to an equivalent two-level system for this resonance are given in Appendix C. We are suggesting here that the I^5 dependence on the shift is merely a corsequence of having chosen a ten-level system.

E. Collisional Effects

The problem of including line-broadening terms can be approached in several ways. The easiest assumes only hard collisions (for our purposes, those which relax an excited state out of the system); in that case our previous results are simply modified by using complex energies. Another way, which we will not puruse, is to start the solution with no relaxation, as used above, and to include relaxation

as a perturbation. This second method requires density matrix formalism in applying perturbation theory. The third method, which we will treat in Section III E2, below, starts with the density matrix and applies weak-field perturbation theory directly. We will briefly mention the hard-collision method in Section III E1 and will concentrate on the direct method in Section III E2, although the treatment of relaxation as a perturbation gives nearly as useful a result. We will not address the problem of collisions which transfer population within the multilevel system, although these could also be treated by appropriate modification of the equations of the system.

1. Hard Collisions

When only hard collisions are present we may keep the Schroedinger equation, Eq. (1), if we allow the diagonal matrix elements to contain imaginary parts. In this case,

$$H_{kk} = E_k - (k-1)\hbar\omega_L + i\Gamma_{kk} \tag{34}$$

and the previous treatment holds. The corresponding relaxation term of the density-matrix element ρ_{jk} is Γ_{jk} which, with these hard collisions, become

$$\Gamma_{jk} = 0.5(\Gamma_{jj} + \Gamma_{kk}). \tag{35}$$

The Stark shift of the upper or lower level n due to the diagram $n \to n \pm 1 \to n$ is

$$\frac{|H_{n,n\pm1}|^2}{\nu - H_{n\pm1,n\pm1}} \quad , \tag{36}$$

and because the diagonal matrix elements are complex, this Stark shift is complex too. As in Eq. (22) this shift adds to H_{nn}, which also has an imaginary part. The total imaginary part of the equivalent two-level Hamiltonian diagonal matrix element corresponding to level n is for $k = n \pm 1$

$$i\Gamma_{nn}[1 + O(\Delta E_s \Gamma_{kk}/\hbar\Omega\Gamma_{nn})] \quad , \tag{37}$$

where ΔE_s is the Stark shift of level n. Usually the correction is small, because $\Delta E_s/\hbar\Omega \sim O(\omega_R/\Omega)^2$, which we have assumed small in the weak-field limit. Consequently, the linewidth of the resonance can be, to good approximation, determined by only Γ_{mm} for $m = n_u, n_L$. When the effective Rabi frequency Ω_R is large compared to $\Gamma_{n_u n_L}/\hbar$ of Eq. (35), Ω_R determines the linewidth. When $\Gamma_{n_u n_L}/\hbar$ is large compared to the Rabi frequency, the Γ determines the width.

Conditions similar to those applied above to the linewidth apply to the Stark shifts. Thus, the corrected Stark shift is

$$\Delta E_s[1 + O(\Gamma_{kk}/\hbar\Omega)] \quad , \tag{38}$$

where ΔE_s is the Stark shift in the absence of relaxation. Because a shift is not significant unless it is greater than the linewidth we may neglect the correction when

$$\text{Max}(\hbar\Omega_R, \Gamma_{nn}) >> \Delta E_s(\Gamma_{kk}/\hbar\Omega) \quad , \tag{39}$$

When $\Gamma_{nn} > \hbar\Omega_R$ the condition is the same as given by Eq. (37). When $\hbar\Omega_R > \Gamma_{nn}$ meeting of the previous condition guarantees Eq. (39).

Lastly, the effective Rabi frequency becomes corrected to

$$\Omega_R[1 + 0\ (\Gamma_{kk}/\hbar\Omega)] \quad , \tag{40}$$

where Ω_R is the Rabi frequency in the absence of relaxation. For this correction to be small we require $\Gamma_{kk} << \hbar\Omega$. If, however, we want to describe the lowest significant-order shift and the shape of the resonance we require the less stringent condition that the change in Rabi frequency be small compared to the linewidth

$$\text{Max}(\Gamma_{nn}, \hbar\Omega_R) >> \Omega_R(\Gamma_{kk}/\Omega) \quad . \tag{41}$$

That is, when $\Gamma_{nn} > \hbar\Omega_R$ we require for an N-photon transition

$$1 >> (\omega_R/\Omega)^N \Gamma_{kk}/\Gamma_{nn} \quad , \tag{42}$$

which usually occurs in the weak-field limit so that this condition is usually met and, thus, as before, Eq. (41) is satisfied.

In summary, we have shown that with hard collisions and a weak field, a description of the resonances at the lowest significant order requires that only the upper and lower relaxation parameters be retained. When, in addition, $\Gamma_{kk} << \hbar\Omega$, the Rabi frequency and Stark shifts may be replaced by their value in the absence of relaxation to lowest significant order.

2. Density Matrix in Weak Fields

When soft and hard collisions are present we must start with the density matrix equations[33]. These equations can be simply written for an N-level atom in terms of our diagrams, but several conventions must be introduced. First, for this purpose only, we represent a pair of arrows going to and from known states by a single bar

(43)

Second, instead of drawing lines for levels, we can represent each level by a point. Thus, the two-level density matrix equations can be written

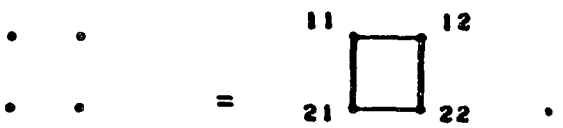

(44)

where the matrix element labels the state. The diagonal matrix element or energy for state jk is $\hbar\Omega_{jk} + i\Gamma_{jk}$.

Likewise, the RHS of the diagram equation for a three-level density-matrix approach is

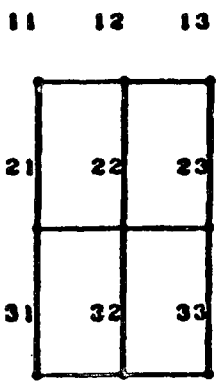

(45)

Additional processes such as spontaneous emission may be simply included, for instance, by terms going from (33) → (22) and from (22) → (11).

The analogue of a Hamiltonian for the density matrix is denoted by H_ρ, which is defined by

$$-i\hbar\partial/\partial t\ \rho_{jk} = \Sigma_{m,n} H_{\rho jk,mn}\rho_{mn} \quad , \tag{46}$$

where H_ρ has nondiagonal matrix elements

$$(H_\rho)_{jk,mn} = \delta_{kn}H_{kj} - \delta_{jm}H_{kn} \quad , \tag{47}$$

and diagonal matrix elements

$$(H_\rho)_{jk,jk} = \hbar\Omega_{jk} + i\Gamma_{jk} \quad . \tag{48}$$

The nondiagonal matrix elements may be simply read off the square diagram by the following rules:

(i) For horizontal transitions, the matrix element for ρ_{ij} to $\rho_{i\ j\pm1}$ is $-H_{i,j\pm1}$.

(ii) For vertical transitions, the matrix element for $\rho_{i\pm1j}$ to ρ_{ij} is $H_{i,\ i\pm1}$.

As an example we may read off the equation

$$-i\hbar\partial/\partial t\ \rho_{22} = i\Gamma_{22}\rho_{22} + H_{12}\rho_{12} - H_{23}\rho_{23} + H_{32}\rho_{32} - H_{21}\rho_{21} \quad . \tag{49}$$

At this point we may apply all our previous rules for treating diagrammatic perturbation theory to our square diagram; however, the problem is intrinsically more difficult. Suppose we consider a transition between levels 1 and M, then the energies (diagonal matrix elements) associated with ρ_{11} and ρ_{MM} are $i\Gamma_{11}$ and $i\Gamma_{MM}$, respectively. The real parts are degenerate, but the imaginary parts are not. The resonance condition $\Omega_{1M} \simeq 0$ also causes ρ_{1M} and ρ_{M1} to have nearly zero real parts. However, because the resonant condition does not enter into the condition on the diagonal elements we must take all diagonal elements as being nearly degenerate. Consequently, we may, by applying

our diagrammatic perturbation theory, reduce the NxN element problem to one that has N+2 elements i.e., $\rho_{11}.\rho_{22}.....\rho_{NN}$ as well as ρ_{1M} and ρ_{M1}. This in itself is a substantial reduction of the problem. An additional assumption i.e., that the problem is reduced to four elements: ρ_{11}, ρ_{MM}, ρ_{1M}, and ρ_{M1}, may be justified <u>a posteriori</u> in certain cases.

Let us apply this technique to a three-level system with a $1 \rightarrow 3$ resonance. The effective Hamiltonian for the system is denoted by H'_{ρ}

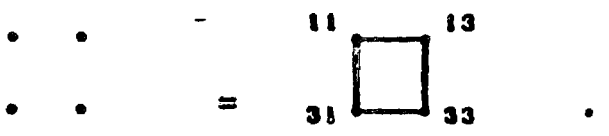

(50)

where using $\mu_{jk} = (\nu - \hbar\Omega_{jk} - i\Gamma_{jk})^{-1}$ we have

$$H'_{\rho_{11,11}} = H_{12}H_{21}(\mu_{21} + \mu_{12})$$

$$H'_{\rho_{33,33}} = H_{32}H_{23}(\mu_{23} + \mu_{32}) \qquad (51)$$

$$H'_{\rho_{13,13}} = H_{32}H_{23}(\mu_{12} + \mu_{23})$$

$$H'_{\rho_{31,31}} = H_{32}H_{23}(\mu_{21} + \mu_{32})$$

and when the off-diagonal matrix elements are real, as in our cases,

$$
\begin{aligned}
H'_{\rho_{13},11} &= H'_{\rho_{11},13} = H_{12}H_{23}\mu_{12} \\
H'_{\rho_{31},11} &= H'_{\rho_{11},31} = H_{12}H_{23}\mu_{21} \\
H'_{\rho_{13},33} &= H'_{\rho_{33},13} = H_{12}H_{23}\mu_{23} \\
H'_{\rho_{31},33} &= H'_{\rho_{33},31} = H_{12}H_{23}\mu_{32} \ .
\end{aligned}
\tag{52}
$$

The value assumed by ν is small, as before, compared to the detunings so that it may be dropped. In addition, when

$$
|\hbar\Omega_{32}| >> \Gamma_{23}, \ |\hbar\Omega_{12}| >> \Gamma_{12} \ , \tag{53}
$$

we have

$$
H'_{\rho_{11},11} = H'_{\rho_{33},33} \cong 0 \ . \tag{54}
$$

and

$$H'_{\rho_{13},11} \cong -H'_{\rho_{31},11} = -A \ , \qquad (55)$$

$$H'_{\rho_{13},33} \cong -H'_{\rho_{31},33} \equiv B \ .$$

The resonance condition makes $\Omega_{12} \sim \Omega_{23}$ so that $B \sim A$, which constitutes the equivalent two-level system

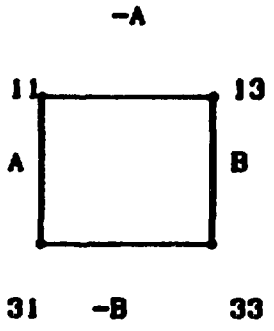

(56)

with diagonal matrix elements for elements 11,13,31,33 of $i\Gamma_{11}$, $i\Gamma_{13} + \hbar\Omega_{13}$, $i\Gamma_{13} + \hbar\Omega_{31}$, $i\Gamma_{33}$, respectively. The effective two-level matrix element H_{12} becomes $H_{12}H_{23}/\hbar\Omega_{21}$.

3. Soft-Collision Limit

In the weak-field density-matrix perturbation theory we require $|\hbar\Omega_{jk}| >> \Gamma_{jk}$ for $j \neq k$. But when the opposite condition occurs and the dephasing or soft-collision terms Γ_{jk} are large compared to the detunings we may still apply weak-field perturbation theory. However, the character of the problem is different. The term weak-field implies that the stimulated emission rates (to be defined below) are also small compared to Γ_{jk}.

In this limit the off-diagonal density-matrix elements that do not connect nearest-neighbor levels are small compared to the nearest-neighbor elements and the diagonal elements. Also the time derivatives of the off-diagonal elements are small and may be neglected. When the off-diagonal terms are replaced in the diagonal equations the following rate equations result

$$\frac{\partial}{\partial t} n_j = -\frac{\Gamma_{jj} n_j}{\hbar} - (n_j - n_{j+1})\,\sigma_{j,j+1}\,I_p - (n_j - n_{j-1})\,\sigma_{jj-1}\,I_p \quad , \tag{57}$$

where

$$n_j = \rho_{jj}, \qquad \sigma_{jk} I_p = \frac{2|H_{jk}|^2 \Gamma_{jk}/\hbar}{(\hbar\Omega_{jk})^2 + \Gamma_{jk}} \tag{58}$$

and subscripted quantities with subscripts of 0 or N+1 are defined to be zero. Here the σ_{jk} term may be thought of as the stimulated cross section for j to k, where I_p is the number of photons per unit area per

unit time. The important aspect of this limiting case is that multiple-photon resonances, which require off-diagonal $\rho_{jk} \neq 0(1)$, do not occur. Rather, stepwise processes dominate.

To understand the nature of this rate-equation solution, we may consider an on-resonance harmonic oscillator with $\Gamma_{jj} = \hbar/T_1$ and with a finite number of states N. In Appendix D we show that system , if initially in the ground state, may be expressed for all time in terms of Laguerre polynomials

$$n_{j+1}(t) = \sum_{k=1}^{N} w_k L_j(x_k) \exp[-(\sigma_{12} I_p x_k + T_1^{-1})\, t] \quad . \tag{59}$$

where w_k and x_k are weights and ordinates of a special Laguerre interpolation scheme. In the limit of $N \to \infty$, we show

$$n_{j+1}(t) = \frac{(\sigma_{12} I_p t)^j}{(1 + \sigma_{12} I_p t)^{j+1}} \exp\left(\frac{-t}{T_1}\right) , \tag{60}$$

which implies a constant rate of absorption of energy into the system for times short compared to T_1 because the stored energy of the system is

$$\sum_{j=0}^{\infty} j\hbar\omega_{21} n_{j+1} = \hbar\omega_{21}\sigma_{12} I_p t \exp(-t/T_1). \tag{61}$$

IV. STRONG-FIELD LIMIT

A. Transition From Weak To Strong Fields

We now return to the case where the phase interruption rate is absent or small compared to the detunings, and where multiple-photon resonances exist for weak fields. As we increase the intensity the multiple-photon resonance lines begin to overlap, and our simple picture of an effective two-level system breaks down.

The effect of overlapping resonances can be seen in Fig. 8 . Here we plot the maximum population of level 6 over time as a function of frequency. We are at an intensity of $4GW/cm^2$ giving $\omega_R = 1.16\Delta$ and we see the usual five-photon resonance of $1 \rightarrow 6$. At $\omega_L = \omega_{21} - 1.5\Delta$ we see an additional resonance that is predominately a $1 \rightarrow 5$ resonance followed by a $5 \rightarrow 6$ significantly broadened single-photon resonance (it has also been affected by multiple-photon resonances). The overlap of the $5 \rightarrow 6$ and the $1 \rightarrow 5$ resonances then accounts for the structure we observe. In the dashed curves in Fig. 8 we show two single-photon resonances: the $1 \rightarrow 2$ and the $5 \rightarrow 6$. The $5 \rightarrow 6$ curve is computed by starting the atom in level 5 and looking at the maximum population with respect to time occurring in level 6.

As the intensity increases, the structure of the solid curve of Fig. 8 becomes wider and overlaps so that more and more resonances are simultaneously important. In the limit of very high intensities, all resonances are important, all lines overlap, and we have the equivalent of an on-resonance harmonic oscillator. The similarity in the early time behavior of an anharmonic oscillator near the high-intensity limit and in that of a finite-level and infinite-level harmonic oscillator is shown in Fig. 9 .

The shapes of the early time curves agree well, where $\omega_R = 3.36\Delta$ and $I = 40GW/cm^2$. The difference in amplitudes of the two curves can be attributed to an effective detuning of the harmonic oscillator. Had the infinite-level harmonic oscillator been detuned by 2Δ (the detuning of our anharmonic oscillator), the amplitude would have dropped to ~ 4 at $\omega_R t \sim 6$. As ω_R is increased the effect of the

detuning becomes less pronounced and the anharmonic curve approaches the ten-level harmonic-oscillator curve. Because the high-intensity limit of the anharmonic oscillator is the harmonic oscillator, we will examine this case in detail below.

B. The Finite-Level Harmonic Oscillator

The on-resonance harmonic oscillator is a special case of our Hamiltonian subject to analytical treatment. The harmonic-oscillator matrix elements are proportinal to $n^{1/2}$. In this case the eigenvalues and eigenvectors can be solved exactly.[34] The eigenvalue and eigenvector condition may be written as

$$\begin{vmatrix} -\lambda & y & & & & \\ y & -\lambda & \sqrt{2}y & & & \\ & \sqrt{2}y & -\lambda & \sqrt{3}y & & \\ & & & & & \\ & & & \sqrt{N-1}y & -\lambda & \sqrt{N} \end{vmatrix} \begin{vmatrix} a_1 \\ a_2 \\ a_3 \\ \\ a_N \end{vmatrix} = 0 \ , \tag{62}$$

where

$$y = 0.5\hbar\omega_R, \ \omega_R = \mu_{12} \cdot E/\hbar \ , \tag{63}$$

and ω_R is the Rabi-frequency.

This equation is supplemented by the boundary condition $a_n(t=0) = \delta_{no}$ and is solved by

$$a_{n+1}(t) = \sum_{1}^{N} (\pi n!)^{-1/2} W_m He_n(X_m 2^{1/2}) \exp(i2^{1/2} X_m yt/\hbar) \quad . \tag{64}$$

The details of this solution are given in Appendix E. Here He_n are the modified Hermite polynomials, and X_m and W_m are the usual hermitian ordinates and weights respectively. The following is an N-term Hermite approximation to the integral.

$$\hat{a}^{\infty}_{n+1}(t) = (\pi n!)^{-1/2} \int_{-\infty}^{\infty} dx \exp(-x^2) He_n(2^{1/2} x) \exp(i2^{1/2} xyt/\hbar) \quad . \tag{65}$$

Thus, the N-term Hermite approximation to the above integral is the exact solution to an N-level system. Letting $N \to \infty$ we conclude that Eq. (65) is the exact solution to the on-resonance infinite harmonic oscillator problem.

This integral can be solved analytically and the result compared to the well-known solution to the infinite-level harmonic oscillator system. From Gradshteyn and Ryzhik[35], we find

$$\int_{-\infty}^{\infty} dx \exp(-x^2) He_n(2^{1/2} x) \exp(i2\alpha x) = i^n \pi^{1/2} (2^{1/2} \alpha)^n \exp(-\alpha^2). \tag{66}$$

Letting $\alpha = yt/\hbar\sqrt{2}$, we find

$$a_{n+1}(t) = \frac{(i\alpha\sqrt{2})^n \exp(-\alpha^2)}{\sqrt{n!}} \quad . \tag{67}$$

This result gives the well-known Poisson distribution of populations with the mean quantum number $2\alpha^2 = (\omega_R t/2)^2$. The absorbed energy of this system thus varies quadratically in time. This behavior contrasts with the linear time dependence we found in the rate-equation limit. In Fig. (10 we see the time dependence of a ten-level harmonic oscillator. The population acts like a pulse that moves upward and to the right and is reflected from the upper level.

C. Equal-Matrix Elements

The harmonic oscillator with equal-matrix elements between adjacent transitions is another system subject to analytical treatment.[34] The method of solution is similar to that for the usual harmonic oscillator with matrix elements proportional to $n^{1/2}$. Nevertheless, the results differ in important aspects.

In this case the eigenvalue and eigenvector conditions are given by

$$\begin{vmatrix} -\lambda & y & & & & \\ y & -\lambda & y & & & \\ & y & -\lambda & y & & \\ & & & y & -\lambda & y \end{vmatrix} \begin{vmatrix} a_1 \\ a_2 \\ a_3 \\ a_N \end{vmatrix} = 0 \quad , \tag{68}$$

where y was previously defined in Eq. (63). The initial conditions are $a_n(o) = \delta_{n1}$ and the solution given in Appendix F is

$$a_n(t) = (2/\pi) \sum_{1}^{N} w_m U_n(x_m) \exp(2iytx_m/\hbar) \quad , \tag{69}$$

where U_n are Tschebyscheff polynomials of the second kind, and where w_m and x_m are the weights and ordinates of these orthogonal polynomials. We also show in Appendix F that in the limit of $N \to \infty$, we get the Bessel-function expression

$$a_{n+1}(t) = J_n(2yt) + J_{n+2}(2yt) \quad . \tag{70}$$

It may be verified that $\Sigma |a_n|^2 = 1$, and numerical evaluation gives a time dependence of the energy absorbed (in quanta) at long times of

$$\sum n|a_{n+1}|^2 \cong \frac{5}{\pi} (2yt)^{-1} + 2 + \frac{8}{3\pi} 2yt \quad , \tag{71}$$

which is accurate to 4 figures for $2yt > 6$ and is 0.1% high at $2yt = 4$ and 8% high at $2yt = 1$. The form was tested up to $2yt = 100$.

As we would expect, the above nearly linear rate of absorption of energy is slower than if the matrix elements are proportional to $n^{1/2}$. It has the same linear form at large times as the rate-equation limit, but the constants of proportionality are different. These results imply that in the high-field limit of a system having equal matrix elements, the absorbed energy will increase nearly linearly in time initially rather than quadratically as in Fig. 9.

ACKNOWLEDGMENTS

We gratefully acknowledge helpful discussions with Albert Petschek of New Mexico Institute of Mining Technology and Bernard Lippman of New York University.

REFERENCES

1. M. Goppert-Mayer. Ann d. Phys. 9, 273 (1931).

2. C. Besset, J. Horowits, A. Messiah, and J. Winter, J. Phys. Radium, Paris 15, (1954).

3. H. Salwen, Phys. Rev.99, 1274 (1955).

4. J. Shirley, Phys. Rev. 138. B979 (1965).

5. R. Braunstein, Phys. Rev 125, 475 (1962).

6. D. Hodgkinson and J. S. Briggs, Chem. Phys. Let. 43 451 (1973).

7. J. Stone, E. Thiele, and M. Goodman, J. Chem. Phys. 59, 2909 (1973).

8. V. Derbov, M. Kovner. and S. Potapov, Sov. J. Quantum Elect. 5, 379 (1975).

9. R. Gilmore, C. Bowden, and L. Narducci, Phys. Rev. A12, 1019 (1975).

10. J. Stone, E. Thiele, and M. Goodman, J. Chem. Phys. 63, 2936 (1975).

11. V. Akulin, S. Alimpiev, N. Karlov, and L. Shelepin, JETP 42, 427 (1976).

12. J. Ackerhalt and J. Eberly, Phys. Rev. A14, 1705 (1976).

13. T. P. Cotter, W. Fuss, K. L. Kompa, and Stafast, Opts. Comm. 18, 220 (1976).

14. W. Bruland, M. Fayer, and C Harris, Phys. Rev. A13, 383 (1976).

15. T. Einwohner, J. Wong, and J. Garrison, Phys. Rev. A14, 1452 (1976).

16. C. J. Elliott and B. J. Feldman, Opts. Comm. 18, 35 (1976).

17. F. Faisal, Opts. Comm. 17, 247 (1976).

18. J. Hougen, J. Chem. Phys. 65. 1035 (1976).

19. D. Larsen and N. Bloembergen, Opts. Comm. 17, 254 (1976).

20. V. S. Letokhov and A. Makarov, "Coherent Excitation of Multilevel Molecular Systems in Intense Quasi-resonant Laser IR Field," USSR, Akademgorodok, Podol'skii-Rayon, Moscow (1976).

21. S. Mukamel and J. Jortner, Chem. Phys. Lett. 40, 150 (1976).

22. L. Rosenberg, Phys. Rev. A14, 1137 (1976).

23. J. Stone and M. Goodman, Phys. Rev. A14, 380 (1976).

24. J. Stone, M. Goodman, and D. Dows, Chem. Phys. Lett. 44, 411 (1976).

25. J. Wong, J. Garrison, and T. Einwohner, Phys. Rev. A13, 674 (1976).

26. D. Grischkowsky, M. Loy, and P. Liao, Phys. Rev. A12, 2514 (1975).

27. F. Block and A. Siegert, Phys. Rev. 57, 522 (1940).

28. The three-level prototype, which forms the subject for Section III-A, has been treated by a number of authors, e.g. Ref. 26, including the recent work of Shore and Ackerhalt, Phys. Rev. A15, 1640 and A16, 277 (1977).

29. I. Rabi, Phys. Rev. 51, GS2 (1937).

30. J. Schwinger, "Lectures on Nuclear Physics", Harvard University (1947).

31. W. Heitler, "The Quantum Theory of Radiation", (Oxford University Press, London (1954), 3rd ed. p. 145.

32. J. F. Ward, Rev. Mod. Phys. 37, 1 (1963).

33. L. Wilcox and W. E. Lamb, Jr.. Phys. Rev. 119, 1915 (1960).

34. B. J. Feldman and C. J. Elliott, Bull. Amer. Phy. Soc. 20, 1282 (1975), see also V. S. Lethokov and A. A. Makarov, opts. Comm. 17, 250 (1976).

35. I. S. Gradshteyn and I. M. Ryzhek, "Table of integrals, Series, and Products, Academic Press, New York (1965).

FIGURES

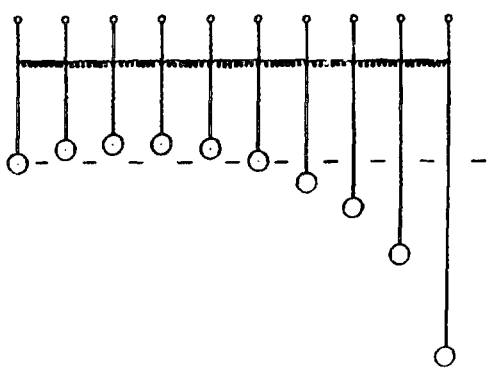

Fig. 1.
Coupled pendulums showing a near resonance between the first and sixth pendulums

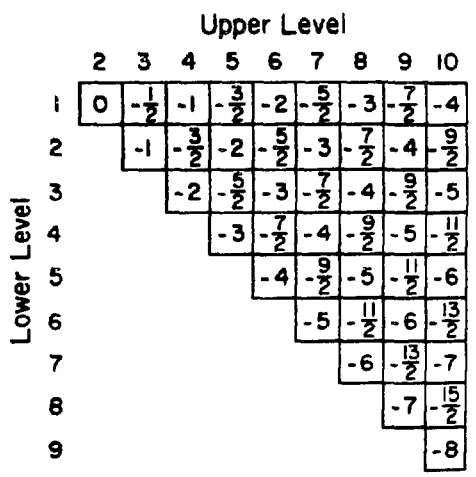

Fig. 2.
Resonance displacements in anharmonic units neglecting Stark shifts.

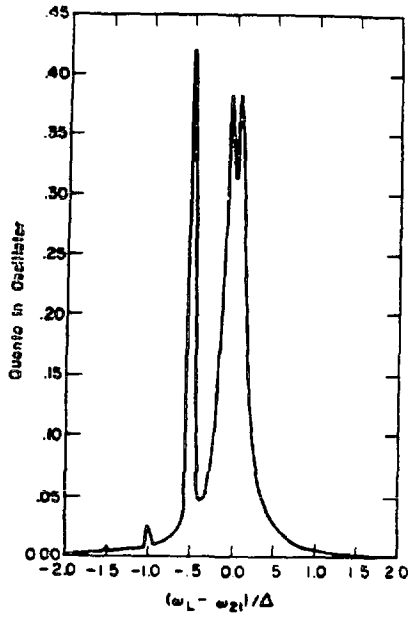

Fig. 3.
Low-intensity resonances with ω_R = 0.116 D.

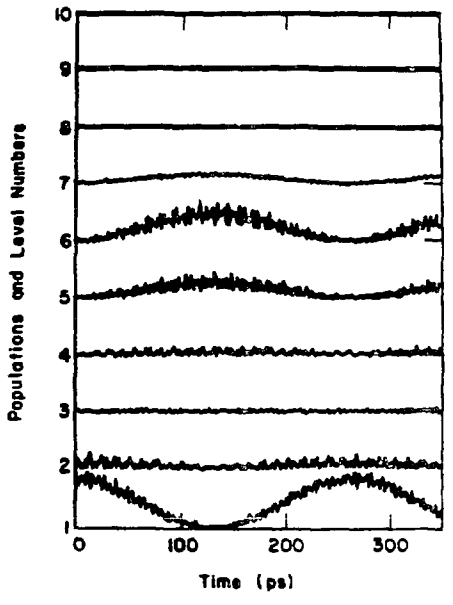

Fig. 5.
Time histories showing a $1 \rightarrow 6$ resonance. The population of level n is plotted between n and n + 1.

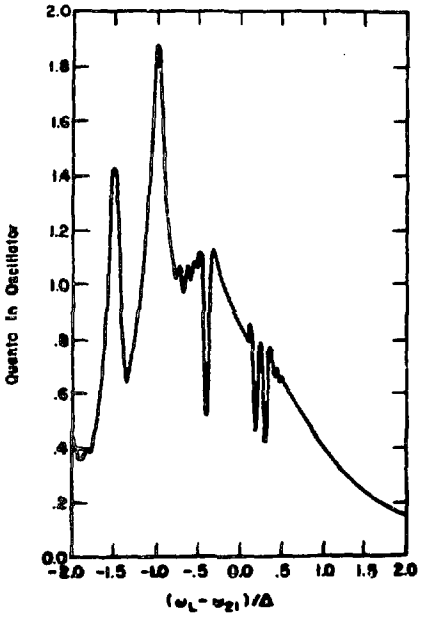

Fig. 4.
High-intensity resonances with ω_R = 1.16 D.

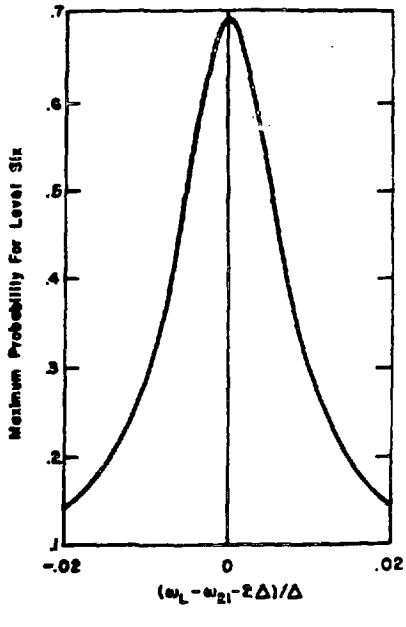

Fig. 6.
Line shape of the $1 \rightarrow 6$ resonance.

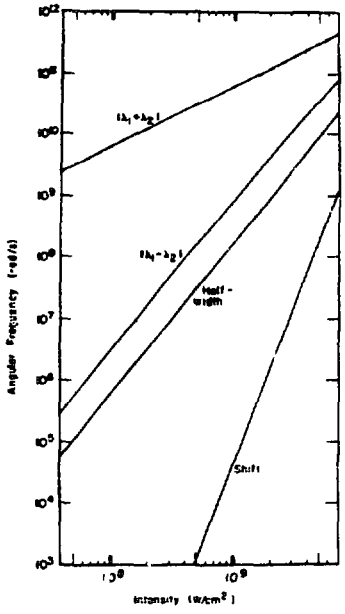

Fig. 7.
Comparison of shifts, widths, and eigenvalues for a ten-level system with a 1 → 6 resonance.

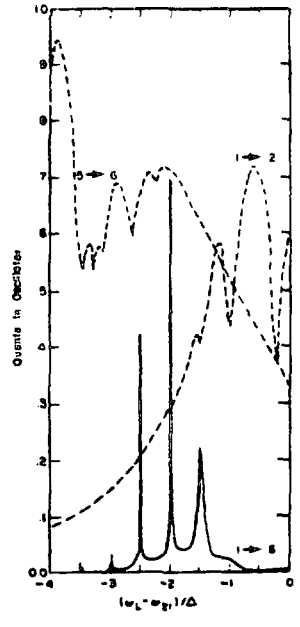

Fig. 8.
Multiple-photon resonances as the weak-field limit is beginning to break down.

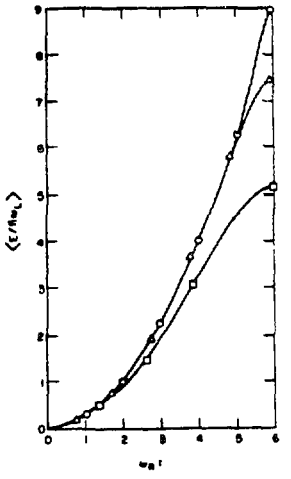

Fig. 9.
Comparison of energies of the on-resonance harmonic oscillator and a high-field case of the anharmonic oscillator. The three curves are: anharmonic oscillator at $\omega_R = 3.36\ \Delta$; Δ 10-level harmonic oscillator, 0-infinite level harmonic oscillator.

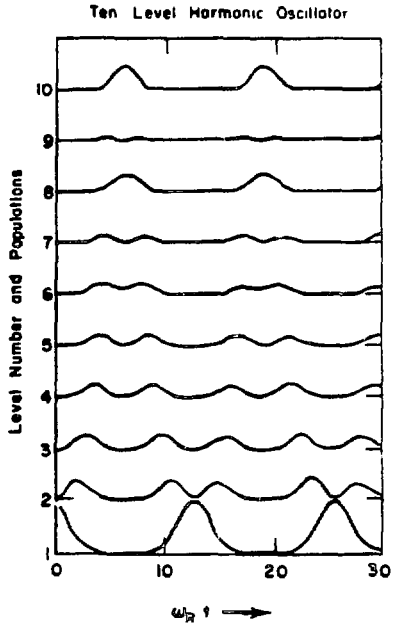

Fig. 10.
Time dependence of harmonic-oscillator populations.

APPENDIX A

THE ROTATING-WAVE APPROXIMATION

The rotating-wave approximation (RWA) applies to periodic Hamiltonians, in particular, of the type

$$-i\hbar\partial\psi/\partial t = (H_0 + H_1\cos\omega t)\psi \quad , \tag{A1}$$

where H_0 and H_1 are time-independent and H_1 has no diagonal terms. We write

$$\psi = \sum_{-\infty}^{\infty} \psi_n(t)\exp(i\omega nt) \quad . \tag{A2}$$

Using Eq. (A2) in Eq. (A1) and equating like frequency components, we have

$$-i\hbar\partial\psi_n(t)/\partial t = (H_0 - \hbar\omega n)\psi_n + H_1(\psi_{n-1} + \psi_{n+1})/2 \quad . \tag{A3}$$

If we introduce two subscript operators a^+ and a^- so that

$$a^+\psi_n = \psi_{n+1} \text{ and } a^-\psi_n = \psi_{n-1} \quad , \tag{A4}$$

we may write

$$-i\hbar\partial\psi_n(t)/\partial t = [H_0 - \hbar\omega n + H_1(a^+ + a^-)/2]\psi_n \quad . \tag{A5}$$

If the eigenvectors of H_0 are denoted by ψ^j

$$H_0\psi^j = E^j\psi^j, \tag{A6}$$

then the eigenvectors of $H_0-\hbar\omega n$ are ψ_n^j with eigenvalues $E^j-\hbar\omega n$

$$(H_0 - \hbar\omega n)\psi_n^j = (E^j - \hbar\omega n)\psi_n^j \quad . \tag{A7}$$

Equation (A5) may now be interpreted in terms of states labeled both with j and n; j labels the atomic state and n the number of photons. In terms of our diagrams we have for a two-level atomic system in which the relative separations on the diagram depend on the value of $\hbar\omega$ and E_2-E_1:

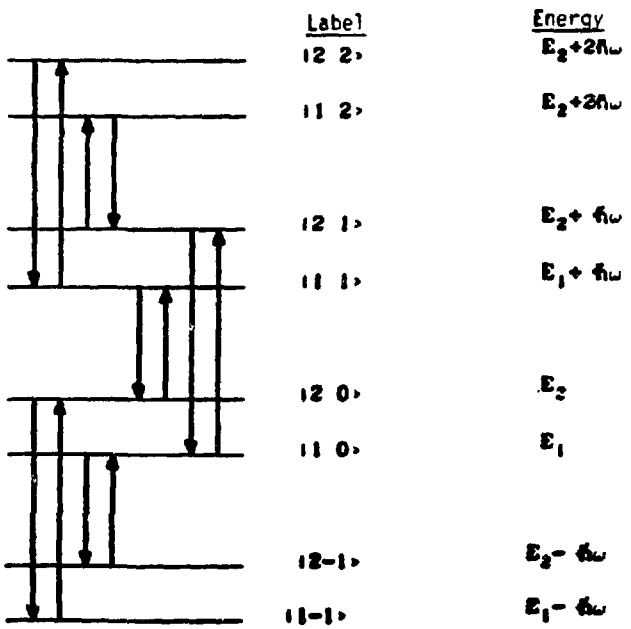

Note that in this semiclassical description, photons with negative energy appear to be required. Salwen[3], however, has shown that these states actually correspond to the atom-plus-many-photons: That is, n+1, n, and n-1 photons correspond to these states. Also, the ψ_n terms have not been renormalized. When $\hbar\omega \sim E_2-E_1$, the states $|11>$ and $|20>$ are nearby each other and all other states are far from these. The rotating-wave approximation chooses only the levels near each other and neglects all others. When antiresonance terms are required for a particular optical effect, the other levels above and below $|20>$ and $|11>$ may be considered (as with a Block-Siegert shift), but because these antiresonant levels are far away one must also consider the other nearby levels of the atom.

The same principle applies if more atomic levels interacting: only the nearby levels are important in RWA. The neglected levels correspond to the antiresonant terms.

APPENDIX B

THE PENDULUM EQUATIONS

The system of pendulums shown in Fig. 1 may be described by the following equations

$$\frac{m\partial^2 x_j}{\partial t^2} = -k_{j-1,j}(x_j - x_{j-1}) - k_{j,j+1}(x_j - x_{j+1}) - mg\frac{x_j}{L_j} \quad , \qquad (B1)$$

for j=1,2,3...N

m=mass of pendulum bobs

L_j=length of j'th pendulum

x_j=displacement of j'th pendulum

k_{jk}=spring constant coupling pendulums j and k

g=gravational acceleration,

where o and N+1 subscripted quantites are set to zero. Assuming an exp(iωt) time dependence the eigenvalue-eigenvector equation can be written

$$\begin{vmatrix} K-K_1 & k_{12} & & & \\ k_{12} & K-K_2 & k_{23} & & \\ & k_{23} & K-K_3 & k_{34} & \\ & & \cdot & & \\ & & & \cdot & \\ & k_{N-2,N-1} & K-k_{N-1} & k_{N-1,N} & \\ & & k_{N-1,N} & K-k_N & \end{vmatrix} \begin{vmatrix} x_1 \\ x_2 \\ \cdot \\ \cdot \\ \cdot \\ x_N \end{vmatrix} = (K-m\omega^2) \begin{vmatrix} x_1 \\ x_2 \\ \cdot \\ \cdot \\ \cdot \\ x_N \end{vmatrix} \qquad \text{(B2)}$$

where $K_j=(mg/L_j) + k_{j,j+1} + k_{j-1,j}$ and where we have added a diagonal K-term to each side of the equation. Equation (B2) is equivalent to Eq. (1) of the text with the substitutions Eqs. (B3), (B4), and (B7) where

$$k_{j,j+1} = \mu_{j,j+1} \cdot \mathcal{E} \quad , \qquad \text{(B3)}$$

and

$$K-K_j = E_j - (j-1)\hbar\omega_L \quad , \qquad \text{(B4)}$$

or

$$L_j = \frac{mg}{K - E_j + (j-1)\hbar\omega_L - k_{j,j+1} - k_{j-1,j}} \qquad \text{(B5)}$$

To keep the denominator finite and positive, we choose the constant K to be large. Note that K in the pendulum equation defines the energy of the oscillator so that all oscillator energies are negative. The m'th pair of eigenvalues of the pendulums is then given by

$$\omega_n = \pm\left(\frac{K - \lambda_n}{m}\right)^{1/2} , \tag{B6}$$

or, conversely,

$$\lambda_n = K - m\omega_n^2 . \tag{B7}$$

In practice K is always larger than λ_n so that the resulting ω_ns are real.

APPENDIX C

TEN-LEVEL SYSTEM

In Sec. III we gave general rules that allowed analysis of an N-level system. To show the power of the diagrammatic perturbation theory we apply it here to a $1 \rightarrow 6$ transition of a quadratically anharmonic 10-level system. Numerical calculations for this system were presented in Fig. 7 and these calculations are done analytically here.

We write the diagram equation in terms of the detuning parameter Ω_{61}. When $\Omega_{61}=0$, level 6 and level 1, in the absence of Stark shifts, would be in resonance for a five-photon transition.

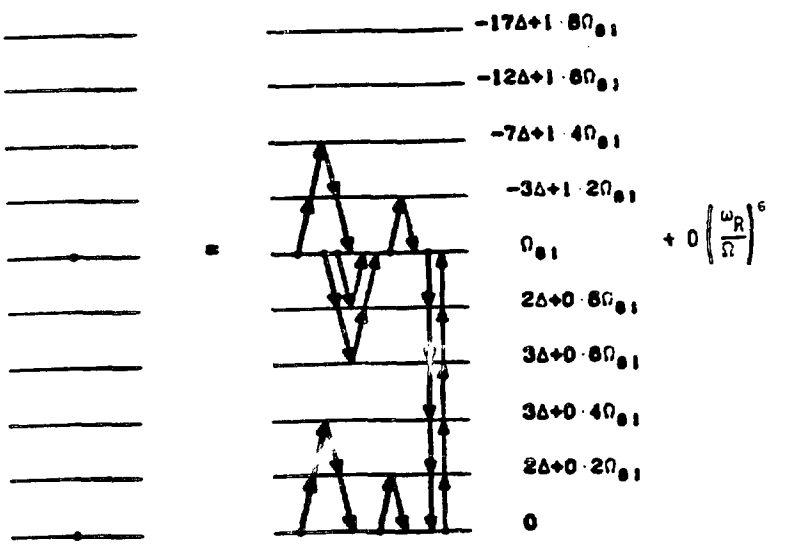

(C1)

The frequencies appearing to the right are computed by expressing $H_{jj}/\hbar$ of Eq. (28) in terms of $H_{66}/\hbar=\Omega_{61}$.

The matrix equation for the equivalent two-level system corresponding to Eq. (C1) is then, by our rules,

$$\hbar \begin{vmatrix} \Omega_{61} + E_{S6} & \Omega_R/2 \\ \Omega_R/2 & E_{S1} \end{vmatrix} \begin{vmatrix} a_6 \\ a_1 \end{vmatrix} = \hbar\nu \begin{vmatrix} a_6 \\ a_1 \end{vmatrix} , \qquad \text{(C2)}$$

where

$$\frac{\Omega_R}{2} = \frac{(5!)^{1/2}\omega_R^5}{32D_2D_3D_4D_5} , \quad E_{S6} = \left(\frac{6}{D_7} + \frac{5}{D_5}\right)\frac{\omega_R^2}{4} + \left(\frac{42}{D_7^2 D_6} + \frac{20}{D_5^2 D_4}\right)\frac{\omega_R^4}{16} \qquad \text{(C3)}$$

$$E_{S1} = \frac{\omega_R^2}{4D_2} + \frac{\omega_R^4}{8D_2^2D_3} , \qquad \text{(C4)}$$

and where

$$D_k = \nu - H_{kk}/\hbar \tag{C5}$$

as for example $D_2 = \nu - 2\Delta - (\Omega_{61}/5)$.

The expression for Ω_R is fifth-order in the field and, thus, ν and Ω_{61} may be neglected compared to -2Δ and -3Δ in this equation. The expressions for the Stark shifts E_{s2} and E_{s6} are lower-order in the field than Ω_R, and in these expressions we cannot drop ν nor Ω as we could in the three-and four-level examples.

Solution of the eigenvalue problem gives rise to two eigenvalues, ν_+ and ν_-, where

$$\nu_+ + \nu_- = E_{s1} + E_{s6} + \Omega_{61} , \tag{C6}$$

$$\nu_+ - \nu_- = [(\Omega_{61} + E_{s1} - E_{s6})^2 + \Omega_R^2]^{1/2} \tag{C7}$$

To demonstrate the equivalence to a two-level system we choose

$$\Omega_{61} + E_{s1} - E_{s6} \equiv O(\Omega_R). \tag{C8}$$

In this case,

$$\nu_{\pm} = E_{s1} + O(\Omega_R). \tag{C9}$$

If we use $\nu = E_{s1}$ and $\Omega_{61} = E_{s1} - E_{s6}$ in the expressions for E_{s1} and E_{s6} in Eq. (C3) the error we commit is seventh-order in the field, less than the error in the approximation of Eq. (C1). Replacing ν and Ω_{61} with these values we find

$$E_{s6}/\Delta = E_{s1}/\Delta = -(\omega_R/\Delta)^2/8 - (\omega_R/\Delta)^4/384 + O(\omega_R/\Delta)^6 \tag{C10}$$

Equation (C1) is then equivalent to a two-level system with the Stark shifts of Eq. (C10). The condition $\nu \cong E_{s1} \cong E_{s6}$ is equivalent to requiring that the Stark shift associated with the upper and lower levels be used to correct the level energy for computing the self-consistent Stark shifts. Because the upper and lower Stark shifts cancel each other, as in Eq. (C10), the actual shift of the line is small compared to the linewidth.

With sufficient levels N it appears that E_{s1} and E_{s6} cancel each other to any given order. However, with a finite N, the $6 \rightarrow N + 1 \rightarrow 6$ diagram, which does not occur, does not allow cancellation of the associated Stark shift. For N=10, $6 \rightarrow 11 \rightarrow 6$ is a tenth-order process so that the resultant shift too, is a tenth order process; had 11 levels been included in the model the line shift would have been twelveth-order. A tenth-order process is observed in Fig. 7 .

APPENDIX D

THE RATE-EQUATION LIMIT

We will show that Eq. (57) has the solution given in Eq. (59), and also that Eq. (60) follows. Now Eq. (57) can be written

$$\begin{vmatrix} R_1 & -\sigma_{12} I_p & & & \\ -\sigma_{12} I_p & R_2 & -\sigma_{23} I_p & & \\ & -\sigma_{23} I_p & R_3 & -\sigma_{23} I_p & \\ & & \cdot & & \\ & & & -\sigma_{N-1,N} I_p & R_N \end{vmatrix} \begin{vmatrix} n_1 \\ n_2 \\ \cdot \\ \cdot \\ n_N \end{vmatrix} = s \begin{vmatrix} n_1 \\ n_2 \\ \cdot \\ \cdot \\ n_N \end{vmatrix} \qquad (D1)$$

where $R_j = \hbar(\sigma_{j,j-1} + \sigma_{j,j+1})I_p + \Gamma_{jj}$ and where we assumed a time dependence of $\exp(-st)$. For our special harmonic-oscillator case $\sigma_{j+1,j}\,\sigma_{j+1,j} = j\sigma_{12}$, $\Gamma_{jj} = \hbar/T_1$, $x = (s-T^{-1})/\sigma_{12}I_p$ so that Eq. (D1) becomes

$$\begin{vmatrix} x-1 & 1 & & & & \\ 1 & x-3 & 2 & & & \\ & \cdot & & & & \\ & & \cdot & & & \\ & & \cdot & & & \\ & & N-2 & x-2N+3 & N-1 & \\ & & & N-1 & x-2N+1 & \end{vmatrix} \begin{vmatrix} n_1 \\ n_2 \\ n_3 \\ \cdot \\ \cdot \\ \cdot \\ n_N \end{vmatrix} = 0 \qquad \text{(D2)}$$

This equation has the Laguerre polynomial solution

$$n_{j+1} = L_j(x)\,, \quad j = 0, 1, 2 \ldots N-1, \qquad \text{(D3)}$$

subject to the requirement for the N'th row, which may be expressed using the Laguerre polynomial recursion relationship,

$$L_N(x) + L_{N+1}(x) = 0 \quad . \tag{D4}$$

This equation has N-roots x_k, which serve to determine the N eigenvalues s_k, where

$$s_k = T_1^{-1} + x_k \sigma_{12} I_p \quad . \tag{D5}$$

The general solution is a superposition of the corresponding eigenvectors

$$n_{j+1}(t) = \Sigma c_k L_j(x_k) \exp(-s_k t), \tag{D6}$$

subject to the boundary condition

$$n_{j+1}(0) = \delta_{j+1,1} \quad . \tag{D7}$$

In addition we have both the orthogonality condition and the weight expression

$$\delta_{j+1,1} = \int_0^\infty \exp(-x) L_j(x) dx = \sum_{k=i}^{N} w_k L_j(x_k), \quad j = 0....N-1 \quad . \tag{D8}$$

Because L_j, for $j < N$, is a polynomial of a degree less than N, Eq. (D8) is exact, and we conclude that $c_k=w_k$. Note that this integration scheme is not the usual Laguerre polynomial scheme which requires that $L_{N+1}(x)=0$; rather, we have our condition of Eq. (D4). Combining the above conclusions we obtain

$$n_{j+1}(t) = \Sigma w_k L_j(x_k) \exp-(T_1^{-1} + \sigma_{12} I_p x_k)t. \tag{D9}$$

and if we allow $N \to \infty$, this N-root approximation to the integral

$$n_{j+1}(t) = \int_0^\infty \exp-[(t/T_1) + (\sigma_{12} I_p t + 1)x] L_j(x)dx \quad , \tag{D10}$$

becomes exact. Integrating Eq. (D10) by the Laplace transformation of L_j yields

$$n_{j+1}(t) = \exp(-t/T_1)\frac{(\sigma_{12} I_p t)^j}{(1 + \sigma_{12} I_p t)^{j+1}} \quad . \tag{D11}$$

APPENDIX E

FINITE-LEVEL HARMONIC OSCILLATOR

Here we will show that Eq. (64) is a solution to Eq. (62). First we note that a solution to Eq. (62), in terms of modified Hermite polynomials, is

$$a_{n+1} = He_n(\lambda/y)(n!)^{-1/2}, \quad n = 1,2,3...N , \tag{E1}$$

where the value of λ must be consistent with the condition of the N'th row, which may be written

$$a_{N+1} = 0 \quad . \tag{E2}$$

This equation has the N-roots $_m$, m=1,2,3...N and the time evolution of the system is given by

$$a_{n+1}(t) = \sum_1^N b_m(n!)^{-1/2} He_n(x_m) \exp(ix_m yt/\hbar) \quad , \tag{E3}$$

and

$$a_{n+1}(0) = \delta_{n+1,1} \quad , \tag{E4}$$

where we have expressed λ_m in terms of the roots x_m of the modified Hermite polynomials with $x_m = \lambda_m/y$.

In addition we have both the orthogonality condition and the weight expression

$$(2\pi)^{1/2}\delta_{j+1,1} = \int_{-0}^{\infty} \exp(-x^2/2)He_j(x)dx = \sum_{1}^{N} w_k He_j(x_k), \qquad (E5)$$

where w_k are the modified Hermite integration weights. These weights and roots for the modified Hermite polynomials are related to the well-known Hermite weights W_k and roots X_k by

$$x_k = \sqrt{2}\, X_k \ , \ w_k = \sqrt{2}\, W_k \qquad (E6)$$

Because of Eq. (E5) and the initial condition we conclude that $b_m = w_m(2\pi)^{-1/2}$ and

$$a_{n+1}(t) = (2\pi n!)^{-1/2}\sum_{1}^{N} w_m He_n(x_m)\, \exp(ix_m ty/\hbar) \ ; \qquad (E7)$$

using Eq. (E6) we arrive at Eq. (64).

APPENDIX F

EQUAL μ CASE

Here we will show that Eq. (69) follows from Eq. (68) and also that it implies Eq. (70). We note that a solution to Eq. (69), in terms of modified Tschebycheff polynomials of the second kind, is

$$a_{n+1} = U_n(\lambda/2y) \ , \tag{F1}$$

where

$$U_n(\cos\theta) = \frac{\sin(n+1)\theta}{\sin\theta} \ . \tag{F2}$$

with

$$a_{N+1} = 0 \ . \tag{F3}$$

The latter condition gives rise to N-roots λ_m which are related to the zeros x_m of the modified Tschebyscheff polynomial of the second kind U_N by $\lambda_m = 2yx_m$. The time evolution of the system is given by

$$a_{n+1}(t) = \sum_{m=1}^{N} A_m U_n(x_m) \exp(2ix_m yt/\hbar) \ , \tag{F4}$$

where

$$a_{n+1}(0) = \delta_{n+1,1} \quad . \tag{F5}$$

The orthogonality and weight expressions may be written

$$\frac{\pi}{2}\,\delta_{n+1,1} = \int_{-1}^{1} dx(1-x^2)^{1/2} U_n(x) = \sum_{m=1}^{N} w_m U_n(x_m), \tag{F6}$$

so that $A_m = 2w_m/\rho$. From which we find

$$a_{n+1}(t) = \frac{2}{\pi} \sum_{1}^{N} w_m U_n(x_m) \exp(2ix_m yt/\hbar) \quad , \tag{F7}$$

which is Eq. (71) and which becomes, as $N \to \infty$,

$$a_{n+1}(t) = \frac{2}{\pi} \int dx U_n(x) \exp(2ixy/\hbar)(1-x^2)^{1/2} \tag{F8}$$

$$= \frac{2}{\pi} \int_{0}^{\pi} d\theta \sin\theta \sin[(n+1)\theta] \exp(i\alpha \cos\theta), \tag{F9}$$

where $\alpha = 2yt/\hbar$. Expanding the products of the sines and using the integral definition of the Bessel function we get

$$a_{n+1}(t) = J_n(\alpha) + J_{n+2}(\alpha) \quad , \tag{F10}$$

which is Eq. (70).